



TAMPEREEN TEKNILLINEN YLIOPISTO
TAMPERE UNIVERSITY OF TECHNOLOGY

CARLOS ANDRÉS BAQUERO BARNETO
PROPAGATION MODELLING OF C BAND DIRECTIONAL
UAV GROUND CONTROL LINKS

Master of Science Thesis

Examiner: Prof. Evgeny Kucheryavy
Examiner and topic approved by the
Faculty Council of the Faculty of
Computing and Electrical Engineering
on 28th February 2018

ABSTRACT

CARLOS ANDRÉS BAQUERO BARNETO: Propagation modelling of C band directional UAV ground control links

Tampere University of Technology

Master of Science Thesis, 69 pages, 3 Appendix pages

February 2018

Master's Degree Programme in Tampere University of Technology

Examiner: Prof. Evgeny Kucheryavy

Keywords: UAV, drone, path loss, propagation, channel modelling, air-to-ground.

Unmanned Aerial Vehicles (UAVs), commonly known as drones, have been widely used in specific military applications since the last century. In the recent years, technological developments regarding main aspects of these vehicles such as batteries, electronics and lightweight materials, have made UAVs more feasible to commercial applications. One of the most remarkable fields where the drones are being applied is for telecommunication applications. Several studies propose systems where the UAVs are used as communication relays. These systems, known as Drone Small Cells (DSCs), act as aerial base stations to support communication networks in high demand situations or when the current ground infrastructures have been damaged. The work done in this Thesis belongs to a project whose main goal is to implement a DSC system.

The system proposed in this project will provide a wireless access point to the clients using a communication relay mounted in an aerial vehicle. The link that connects the terminals of the clients to the UAV is performed with a simple connection that uses omnidirectional antennas. However, the most critical part of this design, is the link between the UAV and the ground station which will connect the system to the backbone network. This link will use antennas with high directivity in order to deploy the aerial access point at longer distances. In this way, this Master Thesis focuses on the characterization of the link channel with more complexity.

This Master Thesis has developed a propagation model intended for air-to-ground communication links. The path loss between a ground station and a UAV can be analysed by means of the implemented propagation model. The measurement equipment has been set and calibrated in advance in order to present the desired path loss information. Based on empirical data obtained in three different LOS scenarios, a comparison is proposed to some well-known state of art models. However, none of the analysed models describes the path loss properly for this type of environment.

Therefore, a new propagation model has been developed by a linear approach which considers a correction factor according to the UAV's height. As the model is based on a set of empirical measurements, it can only be applied in environments with a certain of features. These characteristics are a distance range between 0 and 600 m, a drone antenna height between 7 and 35 m and a carrier frequency of 5580 MHz. The performance and accuracy of the proposed model have been analysed considering a fourth set of measurements deployed with a different drone antenna height.

Con este Trabajo Fin de Máster quiero dar las gracias a todas las personas que han hecho posible que llegue este fin y la vez comienzo de muchas nuevas etapas. A Guille y a mis padres Carmen y Carlos, a los cuales tengo que dar las gracias por ser la mejor familia que podría tener. A Carmen, mi mejor compañera de viajes y aventuras, porque me es imposible imaginar una vida sin tí. A mis abuelos, Cristina, Lorenzo, Manolo y Mercedes los cuales han dejado una huella en mí que nunca se borrará.

CONTENTS

1. Introduction	1
1.1 Motivation and background	1
1.2 Scope and outline of the Thesis	5
2. Theoretical background	6
2.1 Propagation models	9
2.1.1 Ray tracing-based propagation models	11
2.1.2 Empirical and measurements-based propagation models	11
2.2 Least Squares estimation	16
2.2.1 Theory	16
2.2.2 Linear regression case	18
2.3 Haversine formula	21
3. Measurement equipment and tools	22
3.1 Equipment	24
3.1.1 Antennas	24
3.1.2 Additional hardware	27
3.2 Scripts	29
3.2.1 Power measurement script	29
3.2.2 GPS script	32
3.2.3 Haversine script	35
3.3 System setups and procedures	36
3.3.1 Network setup	36
3.3.2 Measurement setup	38
3.3.3 Measurement procedure	40
4. Measurement analysis	42
4.1 Measurement locations and procedures	42
4.2 Elevation profile	45
4.3 Calibration	48

4.4	Measurement results	48
4.5	Propagation models comparison	50
5.	Propagation modelling	53
5.1	Linear regression approach	53
5.2	Effective height correction	56
5.2.1	Slope correction	56
5.2.2	Intercept point correction	57
5.2.3	Proposed path loss model	58
5.3	Proposed model verification	59
5.4	Error analysis	61
6.	Conclusions and future work	65
	Bibliography	67
A.	Appendix	70
A.1	GPS coordinates algorithm	70
A.2	Antenna measurement algorithm	71
A.3	Haversine algorithm	72

LIST OF FIGURES

1.1	Air-to-ground communication system concept.	2
1.2	Misalignment loss due to vertical and horizontal errors.	3
1.3	Block diagram of proposed tracking system.	4
2.1	Determination of deterministic model paths.	7
2.2	First Fresnel zone.	10
2.3	Geometric interpretation of Least Squares method.	18
2.4	Example of linear regression with one input variable.	19
3.1	Methodology block diagram.	23
3.2	Mikrotik LHG 5 azimuth gain pattern.	25
3.3	Mikrotik LHG 5 elevation gain pattern.	25
3.4	Mikrotik SXT Lite5.	26
3.5	Mikrotik SXT Lite5 gain pattern.	27
3.6	Measurement equipment.	28
3.7	Height correction for Haversine algorithm.	36
3.8	IP Network configuration.	37
3.9	Measurement setup.	39
3.10	Battery configuration.	40
4.1	Measurements routes	43
4.2	Real setup used during channel measurements.	44
4.3	Scenario environments.	45

4.4	Elevation profile and first Fresnel zone at scenario A.	46
4.5	Elevation profile and first Fresnel zone at scenario B.	47
4.6	Elevation profile and first Fresnel zone at scenario C.	47
4.7	Received power samples at scenarios A, B and C.	49
4.8	Path loss samples at scenarios A, B and C.	50
4.9	Propagation models comparison with empirical results.	52
5.1	Least Squares approach at different scenarios.	55
5.2	Slope and intercept point estimation using LS method.	58
5.3	Proposed model with different effective antenna height (h_{eff}).	59
5.4	Measurements locations in scenario D with $h_D = 13m$. The figure is extracted from Google Maps [3] with its permission	60
5.5	Elevation profile and first Fresnel zone at scenario D.	60
5.6	Proposed model analysis of scenario D, $h_{eff} = 14.4m$	61
5.7	Proposed model compared to empirical measurements.	62
5.8	Residual plot from predicted model versus measured values.	63
5.9	Probability density of the proposed model residuals.	64

LIST OF TABLES

2.1	Numerical values for the SUI model parameters	14
2.2	Summary of parameters for empirical path loss model	15
2.3	Summary of parameters for empirical NLOS path loss model	16
3.1	Specifications of LHG 5 series	24
3.2	Specifications of SXT Lite5	26
3.3	Specifications of RB951Ui-2HnD router.	27
3.4	Specifications GM-3 N RU300.	29
3.5	Example of <i>range_test_1.txt</i>	32
3.6	Parameters of GNRMC command.	33
3.7	Sub-network IP configuration	37
3.8	Supported voltage of each device.	38
4.1	Summary of the measurement scenarios.	42
4.2	Summary of the calibrated parameters.	48
5.1	Slope and intercept point for LS method	55

LIST OF ABBREVIATIONS AND SYMBOLS

COW	Cell On Wheels
DSC	Drone Small Cell
EIRP	Effective Radiated Power
FS	Free Space
GLONASS	Global Navigation Satellite System
GPS	Global Positioning System
GTD	Geometrical Theory of Diffraction
LTE	Long Term Evolution
LOS	Line Of Sight
LS	Least Squares
NLOS	Non Line Of Sight
NMEA	National Marine Electronics Association
SNR	Signal to Noise Ratio
SUI	Stanford University Interim
UAV	Unmanned Aerial Vehicles
UTD	Uniform Theory of Diffraction

A	effective area in the receiving side
A_s	correction factor of SUI model
c	speed of light
C_h	Hata correction factor
d	distance
$d(n)$	desired response vector
$e_0(n)$	error vector
f	frequency
f_c	carrier frequency
f_0	reference frequency
G_{TX}	transmitting antenna gain
G_{RX}	receiving antenna gain
h_B	base station antenna height
h_{eff}	effective antenna height
$H(f)$	channel response
h_M	mobile station antenna height
h_t	transmitting antenna height
h_r	receiving antenna height
$hav(.)$	Haversine function

L_B	basic path loss
L_{COST}	COST path loss
L_{FS}	free space path loss
L_{Hata}	Hata path loss
L_{2-ray}	2-ray path loss
PL	path loss
PL_0	path loss intercept point
P_{TX}	transmitted power
P_{RX}	received power
R_n	radius of n Fresnel zone
R_1	radius of first Fresnel zone
R^2	coefficient of determination
$v(n)$	vector of observations
w_0	parameter vector
X_f	frequency correction factor for SUI model
X_h	height correction factor for SUI model
X_σ	zero-mean Gaussian random variable with standard deviation σ
y	vector of observations
\hat{y}	vector of predicted values
γ	terrain correction factor for SUI model
σ	standard deviation
∇	gradient of a vector
$(.)^T$	transpose of a matrix or vector
$(.)^{-1}$	inverse of a matrix
$\ \cdot\ $	norm of a vector

1. INTRODUCTION

1.1 Motivation and background

Unmanned Aerial Vehicles (UAVs), commonly known as drones, have been widely used in specific military applications since the last century. These vehicles are pilot-less and non-crewed aircraft with the capability of flight either by remote control or using on-board computers. In the recent years, technological developments regarding main aspects of these vehicles such as batteries, electronics and lightweight materials, have made UAVs more feasible to commercial applications [11]. The most remarkable commercial fields are package delivery, aerial photography, agriculture and pest control, site inspection and surveys, public safety services and telecommunication applications. Estimations predict a significant growth in the market for civil UAVs, which promises to be one of the most incising sectors for the next decade. Non-military UAV market is expected to rise from 2.8 billion market in 2017 to more than quadruple to 11.8 billion by 2026 [14].

This Thesis has target two potential applications where the UAVs are used as communication relays. These systems, known as Drone Small Cells (DSCs), act as aerial base stations to support communication networks in high demand situations or when the current ground infrastructures have been damaged [10]. The base stations that are currently deployed are dimensioned for an estimated number of users. However, during events with agglomerations such as concerts, the mobile networks usually become saturated producing failures in the clients' mobile service. Furthermore, after natural disasters such as floods or tornadoes, mobile communications networks are often damaged, causing many users to be isolated and in danger.

Consequently, this Thesis will be focused on the propagation channel modelling of a DSC system to provide mobile coverage to these saturated and damaged areas using a communication relay by means of a UAV. The proposed solution requires a short time of deployment, the essential feature for the scenarios where is intended for. Additionally, the principal advantage that this system presents is the low price compared to the current alternatives that deploy Cell On Wheels (COW)[22].

The idea of this project is to provide mobile access to the clients using an aerial vehicle which will be connected to the IP network as the regular mobile base stations do. For this purpose, a backbone link is set between the UAV and a ground station which permits to control the autonomous vehicle and manage the data generated by the users. In this way, the drone will fly to the required area establishing the backbone link using an on-board antenna. Then, it will provide mobile coverage to the users with a second antenna. The Fig. 1.1 shows the general concept that this project proposes, explaining how the users of the Service area are connected to the IP network employing the UAV relay.

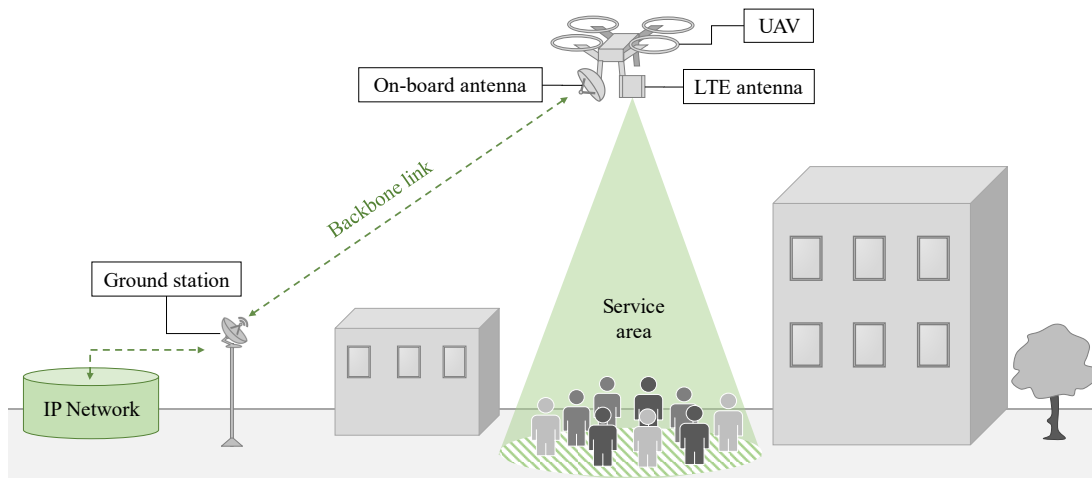


Figure 1.1 Air-to-ground communication system concept.

This approach pretends to deploy the UAV in large areas maintaining the ground station static at the same location. However, as larger the distance between the drone antenna and the ground station is, the quality of the signal received by the antennas is going to be worse. Therefore, to obtain a feasible backbone link at such large distances it is necessary to use antennas with high gain features.

The drone is going to work as a relay which transmits all the traffic demanded by the final users. Therefore, the backbone link will demand an specific equipment to handle such large throughput. This system solves this requirement using antennas which operate at higher frequencies to provide the capacity needed. Specifically, the backbone link is going to be set with two antennas which operate at the C band frequency (4 to 8 GHz) using a carrier frequency around 5.5 GHz. However, the use of high frequencies has the inconvenient of the dependency of the carrier frequency in the path loss. As higher a signal's frequency is, more attenuation the channel produces and consequently the quality of the signal is degraded.

It is plausible that the system needs to deal with the negative effects of providing large distance links with antennas that operate at high frequencies. To solve these disadvantages, the proposed design uses antennas with high gain which mitigate the high path loss that the backbone link presents. To understand how a high gain antenna is implemented it is necessary to explain the dependency of the gain and the beam-width of an antenna. The beam-width is the angle between the half-power (-3 dB) points of the main lobe, when referenced to the peak effective radiated power of the main lobe. It is important to highlight that the beam-width angle is inversely proportional to the antenna gain.

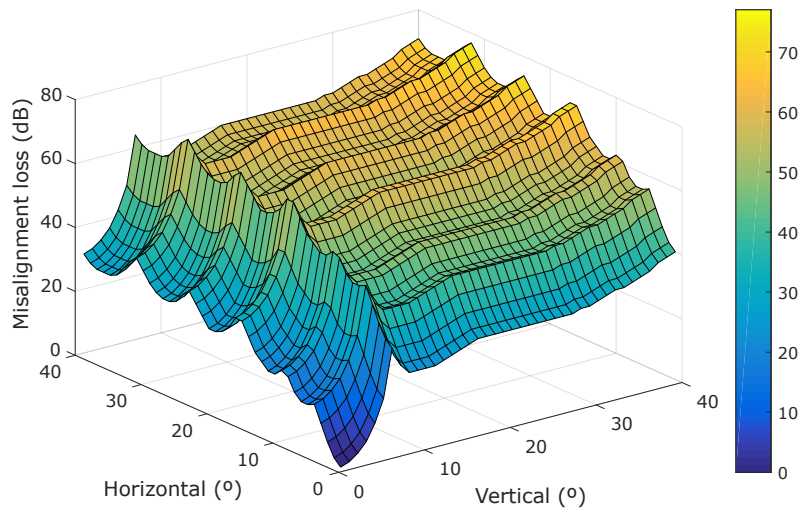


Figure 1.2 Misalignment loss due to vertical and horizontal errors.

It may appear that maximising the gain of an antenna will optimise the performance of a link. However, this may not always be the case. Increasing the gain produces a reduction in the beam-width. This will make pointing the direction of the antenna more critical. The Fig. 1.1 shows the importance of pointing the antennas of link properly. The plot is based on the diagram pattern of the ground station antenna which is used in this project. This figure shows the link losses due to the misalignment of a specific directive antenna. The diagram pattern of this device presents a quite narrow beam-width of 7° and a maximum antenna gain of 24.5 dBi. Using very directive antennas as this one, it can be seen that misalignments of a few degrees either in the vertical or the horizontal axis, cause considerable losses in the link.

A recent review of the literature on this topic found that some research has been done about air-to-ground propagation channels. In [7] the authors presented a path loss model for the radio channel between UAVs and cellular networks. Measurements

were conducted in LTE networks at the 800 MHz frequency band. The results of this article show that path loss exponent decreases as the UAV moves up, approximating free space propagation when the drone is flying around 100 m. A similar study made in [6] models the statistical behaviour of the path loss from a cellular base station toward a UAV. This model is intended to provide a simple prediction of the path loss at 850 MHz that can be useful for the network operators. A key problem with much of the literature in relation to the channel characterization is that they consider very low frequencies compared to the 5 GHz that this system will use. In this way, this Thesis will develop its own propagation model to characterize the backbone link.

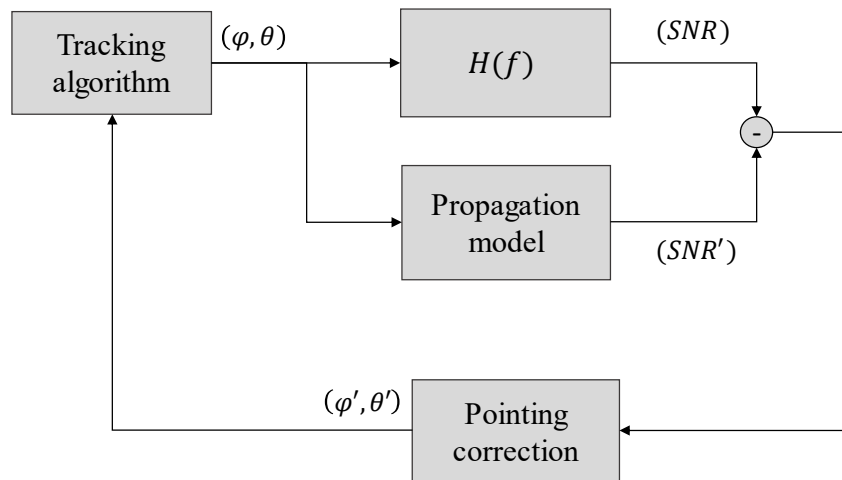


Figure 1.3 Block diagram of proposed tracking system.

The backbone link presented in the system concept of the Fig. 1.1 shows how one of the antennas of that link is mounted on-board of the drone. That means that the position of one of the nodes of the network will be constantly moving, requiring a dynamic tracking system which points both antennas. Therefore, this project proposes the tracking system shown in Fig. 1.3 to point the antennas while the drone is flying. This approach is based on a feedback loop which corrects the antenna misalignment taking into account an approximation of the propagation channel. A tracking algorithm computes the azimuth (ϕ) and elevation (θ) angles of the backbone link antennas taking as reference the coordinates and heights of these antennas. Then, a propagation model estimates how the reception quality should be according to the data given by the tracking algorithm. Finally, a comparison between the received quality (SNR) and the estimated by the propagation model (SNR'), corrects the pointing angles (ϕ' , θ'). This process is it executed iteratively in order to optimize and compensate the misalignment between the antennas of the backbone link.

Consequently, the propagation model is the principal part of the proposed tracking system due to two main reasons:

- The tracking system bases the antennas' pointing angles on the comparison between the measured power strength and the predicted value by the propagation model. The accuracy of the propagation model describing the channel behaviour will determine the precision of pointing both antennas.
- The propagation model will be also used to predict the achievable coverage that the system can provide. It is necessary to analyse the scenario characteristics in advance taking into account the limitations of the equipment used. An accurate propagation model will provide an exact estimation of the system's coverage without the need of deploying the UAV to the desired scenario.

1.2 Scope and outline of the Thesis

The aim of this Master Thesis is the propagation modelling of the most critical link of the system, the backbone link. A propagation model is required to estimate the path loss between the ground station and the UAV. This model should take into account that one of the antennas is going to be placed at large heights as it is on-board of the drone. For this study, the drone height is limited at 30 m due to flight regulations of this kind of aerial vehicles. Another important consideration is that the link uses a carrier frequency of the C band around 5 GHz, frequency that has not been studied for these types of scenarios.

The Master Thesis is organized as follows. In chapter 2, the basics of propagation models and estimation methods are introduced to present a general view of the problem which is addressed. In chapter 3, the measurement equipment and main tools required for the channel characterization are presented. The setups utilized during the measurement campaign as well as the followed methodology are explained in this chapter. The results obtained in different scenarios are shown and compared with alternative propagation models in chapter 4. Chapter 5 proposes a new propagation model based on the measurements made during this project, obtaining a final expression which characterizes the path loss of this system. To conclude, the final remarks and future works are given in chapter 6.

2. THEORETICAL BACKGROUND

As it was explained in the Chapter 1, the most critical part of this design, is the link between the UAV and the ground station which will connect the aerial vehicle to the backbone network as the Fig. 1.1 described. This link will use antennas with high directivity in order to deploy the aerial access point at longer distances. In this way, this project focuses on the characterization of the link channel with more complexity.

When a wireless connection has been established between a transmitting and a receiving antenna, the environment interacts with the electromagnetic waves that travel between both antennas. This interaction produces a reduction in the signal strength that arrives to the receiving antenna that is known as path loss. Therefore, to efficiently set the signal parameters of a wireless communication system, it is necessary to know how the environment affects a specific system.

In the literature, there are several approaches that model the path loss of the channel according to different variables. These estimations of the channel characteristics are known as propagation models. The propagation analysis permits the evaluation of the signal features without the need to perform specific site measurements that require expensive resources. The propagation models can be divided into three main types:

- **Deterministic based propagation models.** These models determine the signal strength taking into account the electromagnetic propagation laws based on very detailed and accurate input parameters. Generally, the deterministic models are based on ray optical theory [23] and some diffraction methods such as the GTD and the UTD. The Geometrical Theory of Diffraction (GTD) explained in [26], describes the diffraction effects when the transmitted signal travels through irregular surfaces that contain discontinuities such as edges and corners. The Uniform Theory of Diffraction (UTD) is an extension of the previous method. Both of these mechanisms are intended for high frequencies and are only applicable when the dimensions of the analysed obstacles are large compared to the wavelength of the signal.

The complexity of a deterministic model will depend on the number of signal contributions that this model includes. Generally, these propagation models consider the combination of the direct ray between both antennas (LOS) with some additional paths that the signal follows such as reflected, diffracted and scattered rays. The Fig. 2.1 shows how the ray tracing is done, considering also the losses due to the reflected and diffracted rays that appear when the signal finds obstacles in its path. As more accurate the model is, more computation sources the model will need. However, this type of propagation model can achieve the most precise results when is fed with enough detailed information about the environment.

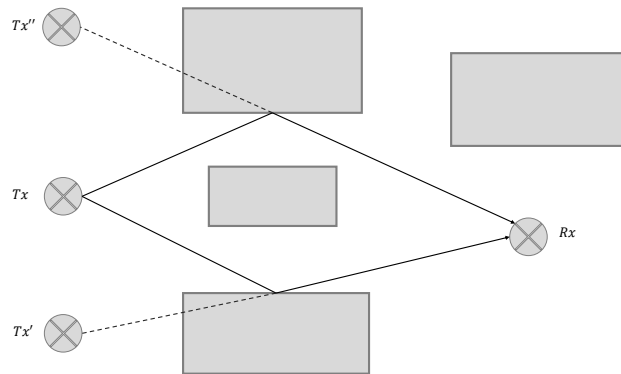


Figure 2.1 Determination of deterministic model paths.

- **Empirical and measurements-based propagation models.** In some cases, it is not possible to characterize the channel behaviour only with a mathematical model as the deterministic models propose. For this reason, another type of propagation models are used based on the practical results obtained in extensive measurement campaigns. This channel characterization is known as empirical models [13], the following are the most significant ones:

- Okumura-Hata Model
- Walfisch-Ikegami Model
- SUI Model

As these models are based on practical measurements that have been made in specific scenarios, their accuracy also depends on the environment where are applied. For instance, the Okumura-Hata model is intended for urban and suburban environments. However, this model is not as precise as the Walfisch-Ikegami approach when is applied to dense-urban environments. This kind of model usually takes notice of several parameters such as effective antenna

height, terrain type, terrain height, carrier frequency, EIRP, etc. Empirical models are simpler and require low computation sources compared with the deterministic ones, but they provide results with lower accuracy.

- **Ray tracing-based propagation models.** These methods are based on the analysis of the different paths that the signal can follow until reaches the receiving antenna. This method is one of the most commonly used approaches in the analysis of propagation models for terrestrial and urban environments.

As a summarize, the deterministic methods are more precise when the environment can be characterized with enough accuracy. However, when the channel is more complex and we need to take into account other effects such as trees, buildings, atmospheric propagation, etc. It is better to use empirical methods. Therefore, both types of methods are useful and in most of the cases complementary. As it was mentioned before, the empirical models provide good accuracy for very specific scenarios. The scenario that this project concerns has two main specifications that the propagation model should take into account.

- **High carrier frequency.** The wireless link between the ground station and the UAV antennas works in the C band, more precisely around the frequency of 5.5 GHz. The high carrier frequency supposes the main problem of this project because there is not any propagation model standardized at this frequency.
- **Variable antenna height.** The antenna mounted in the UAV presents different height depending on the UAV flight altitude. We need to implement a propagation model that takes into account this parameter.

This Theoretical Background chapter will be focused on the study of different propagation models that are going to be compared with some practical measurements in future chapters. The goal of this chapter is to show how a propagation model is defined in order to implement a new empirical propagation model that fulfils these project specifications. Therefore, this chapter is divided into three main blocks. In the first one, several deterministic and empirical models are shown. The second section detail the Least Squares method required to obtain the empirical model from the measurements done in different scenarios. Finally, a section discusses the Haversine formula that is going to be useful for the measurement procedure.

2.1 Propagation models

In this section, some ray tracing-based and empirical methods are analysed, specifying the most important expressions required for their implementation. The idea of this section is to understand how the different parameters such as distance, frequency and antenna height can affect a propagation model.

Firstly, it is necessary to introduce the free space propagation model (FS) which describes the ideal propagation between the transmitting and receiving antennas, assuming that there is only one clear line-of-sight (LOS) path between both devices. The "Standard Definitions of Terms for Antennas" [15], defines "free-space loss" as "The loss between two isotropic radiators in free space, expressed as a power ratio."

This model can only be applied in specific cases when the channel is free of any obstacles. To know in which cases the channel can be approached by a free space model, the concept of Fresnel zones is introduced. According to the electromagnetic theory, a wave is ideally propagated in the whole space. However, the main part of the wave energy goes through the volume known as first Fresnel zone. Consequently, there is a need to keep this zone essentially free of obstructions to obtain a transmission under free space conditions.

To compute the volume of the Fresnel zones, a straight line of length d , should be established between the two antennas of the link. Each Fresnel zone is an ellipsoidal region defined by a radius R_n , where the integer n indicates the Fresnel zone order. The volume enclosed by the ellipsoid defined by $n = 1$ is known as the first Fresnel zone. The volume between this ellipsoid and the ellipsoid defined by $n = 2$ is the second Fresnel zone, etc. The value of the radius R_n depends on the distance where the transmitting and receiving antenna are placed, known as d_1 and d_2 respectively. According to [23] the radius of any Fresnel zone is approached with the following expression, whose parameters are expressed in meters as

$$R_n = \sqrt{\frac{n\lambda d_1 d_2}{d_1 + d_2}}. \quad (2.1)$$

Moreover, the first Fresnel zone can be approximated with the following equation

$$R_1 = 548 \sqrt{\frac{d_1 d_2}{(d_1 + d_2) f}}, \quad (2.2)$$

where the radius R_1 is obtained in meters when the distances to both antennas d_1 and d_2 are expressed in kilometers and the frequency f in MHz. The main parameters

of this equation are graphically shown in Fig. 2.2. The first zone must be free in order to avoid interferences. However, some obstacles in the first Fresnel zone can often be tolerated. Typically, as it is explained in [9], obstacles that block the 20% to 40% of the lower first Fresnel zone are permitted to consider the propagation as free space conditions.

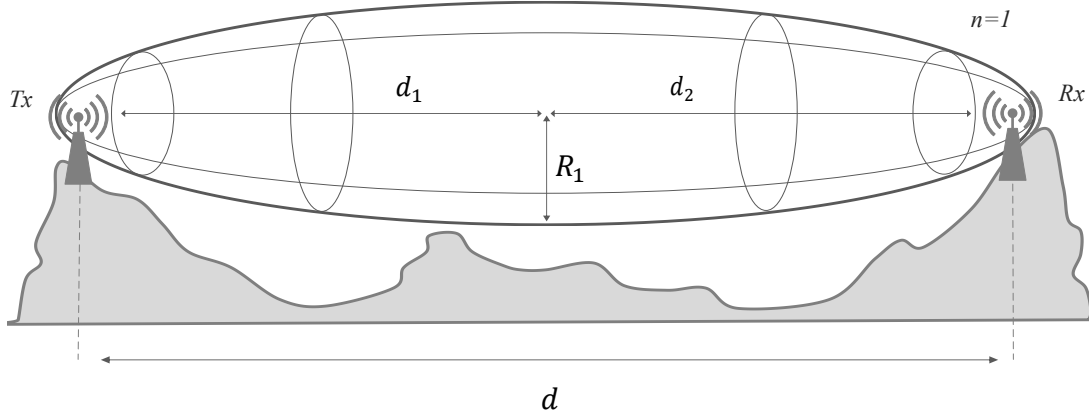


Figure 2.2 First Fresnel zone.

In consequence, if the channel satisfies the free space conditions, the available power P_r at the receiving antenna is computed by the equation 2.3. That depends on the transmitting antenna gain G_t , the provided power by the transmitting antenna P_t , and the effective area A in the receiving side. This area can be approached according to the receiving antenna gain.

$$P_r = \frac{P_t G_t}{4\pi(d)^2} A = \frac{P_t G_t}{4\pi d^2} \left(\frac{\lambda^2 G_r}{4\pi} \right) \quad (2.3)$$

From this equation, the free space or Friis equation is computed as the ratio between P_r and P_t as

$$\frac{P_r}{P_t} = G_t G_r \left(\frac{c}{4\pi f d} \right)^2, \quad (2.4)$$

where c is the velocity propagation ($c = f\lambda$).

According to [23], the propagation loss can be defined in logarithmic units with the expression

$$L_{FS}(dB) = 10 \log_{10} \left(\frac{P_t}{P_r} \right), \quad (2.5)$$

which can be also written as

$$L_{FS}(dB) = -10 \log_{10}(G_t) - 10 \log_{10}(G_r) + 20 \log_{10}(f) + 20 \log_{10}(d) - 147.56. \quad (2.6)$$

Finally, comparing the path loss with the basic path loss L_B between isotropic antennas, the next expression is obtained taking into account that the frequency is usually measured in MHz and the distance in km.

$$L_B(dB) = 32.45 + 20 \log_{10}(f_{MHz}) + 20 \log_{10}(d_{km}). \quad (2.7)$$

2.1.1 Ray tracing-based propagation models

The free space model can be only applied in restricted ideal conditions. However, in most of the practical cases, there are always obstacles or surfaces where the transmitted signal can be reflected. In the reference [23], two scenarios are described. Firstly, propagation over a spherical reflecting surface and secondly, when the distance between the antennas is small enough to consider the reflecting surface flat.

The scenario that concerns to this project has a distance between antennas of a few kilometers. For distances less than a few tens of kilometers, we can assume that the propagation surface is flat, neglecting the curvature effect of Earth. In the receiver side, the direct and the reflected rays arrive with different delays and phases. Depending on the distances between both antennas, the reflected ray will produce either constructive or destructive components regard to the direct ray.

Then the 2-ray path loss model can be simplified in dB units as

$$L_{2\text{-ray}}(dB) = -10 \log_{10} \left\{ \left(\frac{\lambda}{4\pi d} \right)^2 \left[2 \sin \left(\frac{2\pi h_t h_r}{\lambda d} \right) \right]^2 \right\}, \quad (2.8)$$

where λ is the wavelength in meters and h_t and h_r are the heights of the transmitting and receiving antennas in meters.

There are similar ray tracing-based models that try to approach the propagation behaviour with a contribution of more rays. In the article [27], a 3-ray path loss model is presented. This approach includes a third ray formed by the refraction of the transmitted wave in the atmosphere. The 3-ray model is commonly used for predicting near sea surface LOS propagation.

2.1.2 Empirical and measurements-based propagation models

This section describes some empirical models such as COST-231 Hata model, SUI model and some approaches that are intended for the C band where the proposed system will work.

- **COST-231 Hata model**

The COST-231 Hata model extends the Hata model [18] to a higher range of frequencies. Originally, the Hata model predicted the propagation loss for a frequency range up to 1500 MHz. This model is suitable for scenarios with mobile station antenna heights between 1 and 10 m, ground station antenna heights from 30 to 200 m, and link distances from 1 to 10 km.

The Hata model approaches the path loss with the following expression

$$L_{Hata}(dB) = 69.55 + 26.16 \log_{10}(f) - 13.82 \log_{10}(h_B) - C_h + [44.9 - 6.55 \log_{10}(h_B)] \log_{10}(d), \quad (2.9)$$

where C_h is a correction factor that depends on the applied scenario. For small and medium size cities, this factor is

$$C_h = 0.8 + [1.1 \log_{10}(f) - 0.7] h_M - 1.56 \log_{10}(f). \quad (2.10)$$

While in large cities, it follows the expression below

$$C_h = \begin{cases} 8.29 [\log_{10}(1.54h_M)]^2 - 1.1, & \text{if } 150 < f < 200 \\ 3.2 [\log_{10}(11.75h_M)]^2 - 4.97, & \text{if } 200 < f < 1500 \end{cases}. \quad (2.11)$$

The equation 2.9 describes the path loss according to the height of the base station and mobile station antennas in meters, h_B and h_M respectively. The frequency term f , is measured in MHz and the distance d in kilometers.

In addition, the COST-231 Hata model allows using a wider frequency band from 500 MHz to 2000 MHz. As its predecessor, it provides correction factors for three different types of scenarios. The length and height limitations remain constant compared to the regular Hata model. As it is shown in [21], the propagation loss for this model is approximated as

$$L_{COST}(dB) = 46.3 + 33.9 \log_{10}(f) - 13.82 \log_{10}(h_B) + [44.9 - 6.55 \log_{10}(h_B)] \log_{10}(d) + C_h - a(h_M, f). \quad (2.12)$$

In this case the parameter C_h is defined as 0 dB for suburban or open rural environments and 3 dB for urban environments. Additionally, the COST model includes a correction factor a that depends on the frequency and the mobile station height.

For small and medium size cities, this factor is given by the following expression

$$a(h_M, f) = [1.1 \log_{10}(f) - 0.7] h_M - (1.56f - 0.8). \quad (2.13)$$

For large cities, this factor is

$$a(h_M, f) = 3.20 [\log_{10}(11.75h_M)]^2 - 4.97. \quad (2.14)$$

Even this model is not intended for the frequencies that the system will work with, the COST model has been analysed to understand how an empirical model is designed. In the propagation modelling that concerns to this project, a correction factor that depends on the antenna height will be considered as the COST-231 Hata proposes.

- **Stanford University Interim model**

The Stanford University developed an empirical model to bands below 11 GHz. The proposed standard contains channel models known as SUI (Stanford University Interim) propagation models. To calculate the path loss using this approach, the environment is categorised in three different groups with the following features:

- Category A: can be used for hilly areas with moderate or very dense vegetation. This type of terrain presents the highest path loss.
- Category B: is characterized by the hilly terrains with rare vegetation.
- Category C: is suitable for flat terrains or rural with light vegetation, here the path loss is minimum.

The path loss equation with correction factors is presented in [5], and is given by

$$L_{SUI}(dB) = A_s + 10\gamma \log_{10} \left(\frac{d}{d_0} \right) + X_f + X_h + s, \quad (2.15)$$

where d is the distance in meters and d_0 has a constant value of 100 meters. This model is only applicable for distances higher than d_0 . The parameter s is a lognormally distributed factor that is used to consider the shadow facing due to trees and other clutter and has a value between 8.2 dB and 10.6 dB [17]. The parameter A_s depends on the wavelength in meters according to the following expression

$$A_s = 20 \log_{10} \left(\frac{4\pi d_0}{\lambda} \right). \quad (2.16)$$

Additionally, the path loss equation includes a terrain correction factor γ as a function of three variables a , b and c . Moreover, the base station height above ground h_B in meters, should be between 10 and 80 meters. The parameter γ , multiplies the term related with the distance, for this reason it is going to define the slope of the path loss function.

$$\gamma = a - bh_B + \frac{c}{h_B} \quad (2.17)$$

The terrain correction factor can be tuned depending on the terrain category [12] with the values of the Table 2.1.

Table 2.1 Numerical values for the SUI model parameters

Model parameter	Terrain A	Terrain B	Terrain C
a	4.6	4.0	3.6
b(m ⁻¹)	0.0075	0.0065	0.005
c(m)	12.6	17.1	20

The SUI model was defined to the frequency band of 2 GHz. In order to apply this model in higher frequencies, a frequency correction factor X_f is defined depending on the frequency term f in MHz.

$$X_f = 6.0 \log_{10} \left(\frac{f}{2000} \right) \quad (2.18)$$

This model also has a correction factor X_h according to the mobile station height (h_M) in meters. This factor depends on the category of terrain as the following expression shows.

$$X_h = \begin{cases} -10.8 \log_{10} \left(\frac{h_M}{2} \right), & \text{for terrain type A and B} \\ -20 \log_{10} \left(\frac{h_M}{2} \right), & \text{for terrain type C} \end{cases} \quad (2.19)$$

This model proposes an interesting expression which describes the path loss with a linear approach. The SUI model also introduces a random variable in order to consider the shadow fading due to trees and other clutter. The propagation model that is going to be implemented in this project is going to consider as a reference these two features of the SUI model.

- **Empirical path loss model at 5.4 GHz by Hang Zheng**

Nowadays, there is a energetic research about the potential spectrum that the 5th generation mobile networks (5G) will use in a near future. One example of these

studies is the article "Path Loss Models for Urban Macro Cell Scenario at 3.35, 4.9 and 5.4 GHz" by the author Hang Zheng [28], which proposes different path loss models for three different frequency bands. The measurements were performed in a urban environment in the city of Xi'an, China, considering LOS and NLOS scenarios.

In this paper several measurements are approximated using the Least Squares (LS) method to approach the loss behaviour with a linear function. The proposed model has the following expression:

$$PL(d) = PL_0 + 10n \log_{10}(d) + X_\sigma + C \log_{10} \left(\frac{f_c}{f_0} \right). \quad (2.20)$$

The path loss that depends only on the distance in meters, is tuned using some parameters. A constant PL_0 represents the intercept point and the term n describes the slope of the path loss function. Additionally, the log-normal shadow fading is considered by X_σ , a zero- mean Gaussian random variable whose standard deviation is denoted by σ . Moreover, a frequency correction factor is applied with a coefficient C that tunes the ratio f_c/f_0 . If we want to apply this propagation model to a scenario with a carrier frequency f_c , we will need to compare it with a referenced frequency f_0 . The reference frequency that this model comprises is 3.35, 4.9 and 5.4 GHz. The tuning parameters have different values depending on the environment and the carrier frequency as the Table 2.2 shows.

Table 2.2 Summary of parameters for empirical path loss model

f_0	LOS			NLOS		
	n	PL_0	σ	n	PL_0	σ
3.35 GHz	2.00	43.5	2.7	3.23	26.6	1.9
4.9 GHz	2.07	48.6	3.3	3.21	30.8	1.8
5.4 GHz	2.06	50.4	2.8	3.60	24.0	3.2

The coefficient C in LOS environments is fixed with a value of 20, as the free space model defines. However, the model proposes different correction values for scenarios without line of sight as the Table 2.3 proposes.

A new intercept point for NLOS is introduced taking into account the frequency correction.

$$PL'_0 = PL_0 + C \log_{10} \left(\frac{f_c}{f_0} \right) \quad (2.21)$$

This paper shows a good example of a path loss channel characterization, explaining

Table 2.3 Summary of parameters for empirical NLOS path loss model

f_0	NLOS			
	n	PL'_0	σ	C
4.9 GHz	3.23	30.5	1.8	23.4
3.35 GHz	3.22	32.0	3.2	25.9

all the steps that the modelling process should follow. This paper comprises a good explanation of the measurement setup required, as well as the system calibration and the estimation method. For these reasons, it has been taken as a reference during the implementation of this project.

2.2 Least Squares estimation

The Least Squares (LS) method is a widely extended approach for data fitting. The best data fit in the sense of least squares minimizes the distance between the observed data and the model. Due to its deterministic nature, the performance of the least squares approach depends on the size of the dataset. The reference [25] describes this approach, also known as LS method. The LS approach is based on the assumption that there exists a linear model between the observations $v(n)$ and the desired response $d(n)$ as

$$d(n) = w_0^T v(n) + e_0(n) \quad (2.22)$$

where w_0 is the true parameter vector of the model, while e_0 denotes the error between the observations and the desired response.

This section will introduce all the theoretical concepts regarding the LS method implementation, as well as how this sort of estimation problem is solved. Finally, the particular case that concerns to this project will be described.

2.2.1 Theory

In general, given a non-singular matrix $A \in \mathbb{R}^{m \times n}$ and a vector $b \in \mathbb{R}^m$, the equation

$$Ax = b, \quad (2.23)$$

will not have an exact solution in most of the cases. Such system of linear equations will have an exact solution only if the vector b lies on the span of the column space

of the matrix A . However, we can always find a solution x that minimizes the difference between both terms as

$$\|Ax - b\|^2. \quad (2.24)$$

The vector x , that minimizes this difference, is known as the Least Squares (LS) solution and it is written as:

$$Ax =_{LS} b. \quad (2.25)$$

We need to find the vector $x \in \mathbb{R}^n$ that optimizes

$$F(x) = \|Ax - b\|^2 = x^T A^T A x - 2b^T A x + b^T b, \quad (2.26)$$

with a matrix A ($m \times n$), of full rank. This is a problem of convex optimization due to its hessian is the simetric matrix $A^T A$ that is positive definite. As $x \neq 0$,

$$x^T A^T A x = \|Ax\|^2 \geq 0. \quad (2.27)$$

This expression can not be equal zero because A has a full rank and $Ax \neq 0$. As the function F is strictly convex, it has only one local minimum which is also a global solution. To know the value of the global minimum x_{LS} , we calculate the gradient of the function F in that point as

$$\nabla F_{x_{LS}} = 2A^T A x_{LS} - 2A^T b. \quad (2.28)$$

If this expression is equal to zero, the optimum value is computed as

$$A^T (b - A x_{LS}) = 0, \quad (2.29)$$

This can be interpreted as that the error between the linear model and the desired response is orthogonal to the subspace spanned by the column vectors of A , which is known as the orthogonality principle as it can be seen in Fig. 2.3. This expression can be also rewritten as

$$A^T A x_{LS} = A^T b. \quad (2.30)$$

Since $A^T A$ is non-singular, the least squares solution is given by

$$x_{LS} = (A^T A)^{-1} A^T b. \quad (2.31)$$

This problem can be graphically interpreted taking into account the Fig. 2.3. that

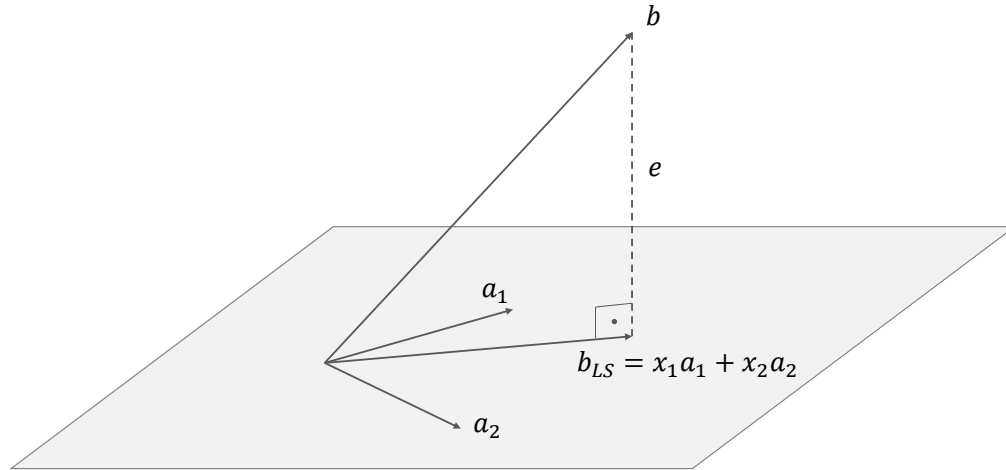


Figure 2.3 Geometric interpretation of Least Squares method.

describes an estimation problem in \mathbb{R}^3 . This problem is set as

$$\begin{bmatrix} a_1 & a_2 \end{bmatrix} \begin{bmatrix} x_1 \\ x_2 \end{bmatrix} =_{LS} b, \quad (2.32)$$

with $a_1, a_2, b \in \mathbb{R}^3$. The plane describes the vectors that can be written as $x_1 a_1 + x_2 a_2$. The vector b represents the LS solution for this estimation problem. However, in general, the system described in equation 2.32 is an overdetermined system, and has not an exact solution in most of the cases, therefore the problem should be treated as an approximation. The final solution will be the projection of the vector b on the subspace spanned by the base vector a_1 and a_2 that is, the column space of the matrix A . Therefore, the LS solution will produce an error e which is orthogonal to the plane where the problem is applied. This error can be written as

$$e = b - (x_1 a_1 + x_2 a_2). \quad (2.33)$$

2.2.2 Linear regression case

In this project, the Least Squares method is only used to model the relationship between the measured losses and some parameters such as the distance and the antenna height. This section explains how a certain number of samples can be approximated with a linear function.

Considering a total of N samples that are shown in the example of Fig. 2.4, their trend can be approximated with a linear regression that considers a set of known

variables y_i , that are related with a set of input variables a_i , for $i = 1, \dots, N$. This regression problem can be formulated according to the equation of a straight line as

$$y = \alpha X + \beta, \quad (2.34)$$

where α indicates the function slope and β its intercept point.

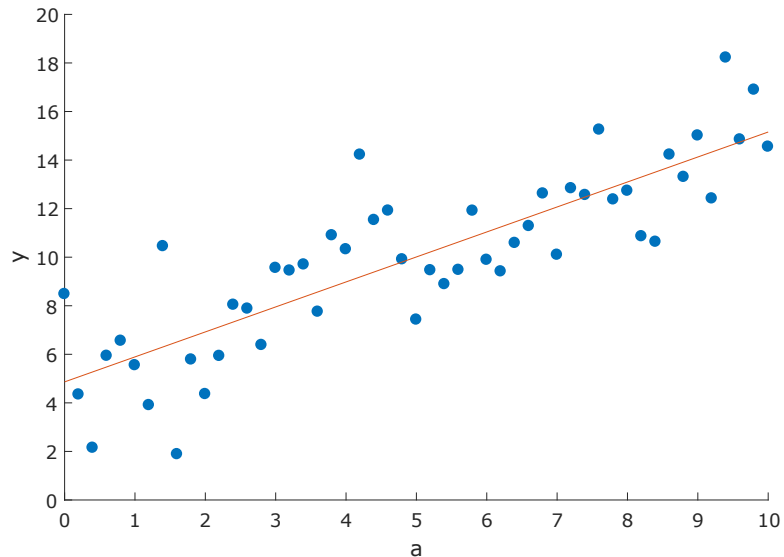


Figure 2.4 Example of linear regression with one input variable.

This problem can be also written as

$$\begin{bmatrix} y_1 \\ \vdots \\ y_N \end{bmatrix} = \begin{bmatrix} a_1 & 1 \\ a_2 & 1 \\ \vdots & \vdots \\ a_N & 1 \end{bmatrix} \begin{bmatrix} \alpha \\ \beta \end{bmatrix}, \quad (2.35)$$

that can be approached according to the Least Squares method as

$$Ax =_{LS} y. \quad (2.36)$$

The optimum value of the vector $x^T = [\alpha \ \beta]$ is calculated as

$$x_{LS} = (A^T A)^{-1} A^T y. \quad (2.37)$$

This LS method will solve the slope and intercept point presented in the equation 2.34. Finally, the function that approaches the set of N samples is presented in red in the Fig. 2.4. Notice that even the LS method tries to minimize the error

according to the expression

$$\|Ax - y\|^2, \quad (2.38)$$

the resulted function is not perfectly exact. To know how accurate this function is, it is necessary to evaluate the error of the regression model. A common way to know how well a regression model fits the observed data used, and consequently the error of that model is using the coefficient of determination [16] or R^2 .

Considering a data set of N known values given by the vector $y = [y_1 \dots y_N]^T$ and their predicted values as $\hat{y} = [\hat{y}_1 \dots \hat{y}_N]^T$. The residuals of this estimation can be expressed as

$$e_i = y_i - \hat{y}_i. \quad (2.39)$$

Knowing that the mean value of the observations is

$$\bar{y} = \frac{1}{N} \sum_{i=1}^N y_i, \quad (2.40)$$

then the deviation of the predicted values respect to the observations can be measured according to following formulas, that take into account the square difference between these values. The coefficient of determination can be computed as

$$R^2 = \frac{\sum_{i=1}^N (\hat{y}_i - \bar{y}_i)^2}{\sum_{i=1}^N (y_i - \bar{y}_i)^2}. \quad (2.41)$$

In a regression model, the coefficient of determination R^2 describes how well the predicted line approximates the real data points. This coefficient has a range between 0 and 1, indicating that the regression line perfectly matches the observations when has a value of 1. Conversely, the worst scenario is represented when R^2 equals zero and the regression does not fix the given data.

Another measure of the accuracy of the model explained in [19] is the standard deviation of the residuals, also known as the "Standard error regression" which can be computed by

$$\sigma = \sqrt{\frac{1}{N-t} \sum_{i=1}^N e_i^2}, \quad (2.42)$$

where t indicates the number of parameters that the regression model estimates. The term e_i refers to the residual of a certain observation.

2.3 Haversine formula

During the path loss modelling, several measurements at different distances are required. To know the distance between two antennas, it is common to use a GPS device which takes the coordinates in every location. Once we have the coordinates from all the positions where the measurements have been made, an algorithm will compute the distance between those coordinates comparing their longitude and latitude information.

Considering the spherical shape of the Earth, the distance between two points placed in its surface can be approximated by the Haversine formula as is explained in [8]. This formula determines the great circle distance between two points on a sphere given their longitudes and latitudes. The Haversine function can be approximated as

$$hav(\theta) = \sin^2\left(\frac{\theta}{2}\right) = \frac{1 - \cos(\theta)}{2} \quad (2.43)$$

Considering an example with two points, P and Q with spherical coordinates (ϕ_1, λ_1) and (ϕ_2, λ_2) . The distance d , between these points, placed on a sphere of radius R , is calculated as

$$hav\left(\frac{d}{r}\right) = hav(\phi_2 - \phi_1) + \cos(\phi_1) \cos(\phi_1) hav(\lambda_2 - \lambda_1). \quad (2.44)$$

Solving the previous equation, the final distance has the following expression

$$d = 2R \arcsin\left(\sqrt{hav(\phi_2 - \phi_1) + \cos(\phi_1) \cos(\phi_1) hav(\lambda_2 - \lambda_1)}\right). \quad (2.45)$$

The Haversine approach considers the Earth as a perfect sphere. However, the Earth has an ellipsoidal geometry whose radius varies depending on the equatorial and the polar locations. If we apply the Haversine model with the mean value usually accepted for the Earth radius of 6,371 km, the accuracy for distances below 1 km is around 3 meters. For this project, this accuracy is more than enough, but we can always apply more precise methods as the Vincenty formula [24] that considers the geodesic distances on ellipsoids, providing an accuracy of millimetres.

3. MEASUREMENT EQUIPMENT AND TOOLS

During the implementation of a propagation model is necessary to follow a specific methodology in order to obtain a successful result. As it was explained in the Chapter 2, a propagation model describes the signal degradation in a certain environment given some variables such as distance link of antennas' height. The proposed propagation model is going to be based on empirical measurements made at different scenarios in order to analyse the effect of the antenna height to the performance of the link.

The methodology diagram followed during this project is shown in Fig. 3.1. It describes an iterative process whose principal goal is to obtain the optimum propagation model which fits the measurement data obtained at different scenarios. The propagation modelling requires measuring two types of data, power strength and coordinates of each location. Once both sources of information are matched, we are able to understand the channel performance compared to the distance of the link. This process needs to be repeated at scenarios with different features in order to analyse them and obtain a satisfactory model which describes the obtained empirical measurements.

Therefore, this chapter presents the equipment required for the channel characterization used in this system. Firstly, the main features of each device are shown emphasizing the ones which concern this project. Secondly, a section will describe the programs that have been implemented in order to automatize the measurement process and save the data related to the power strength and the coordinates. Finally, the system configuration will be presented, showing the measurement setup as well as the steps that an operator should follow during the measurement campaign.

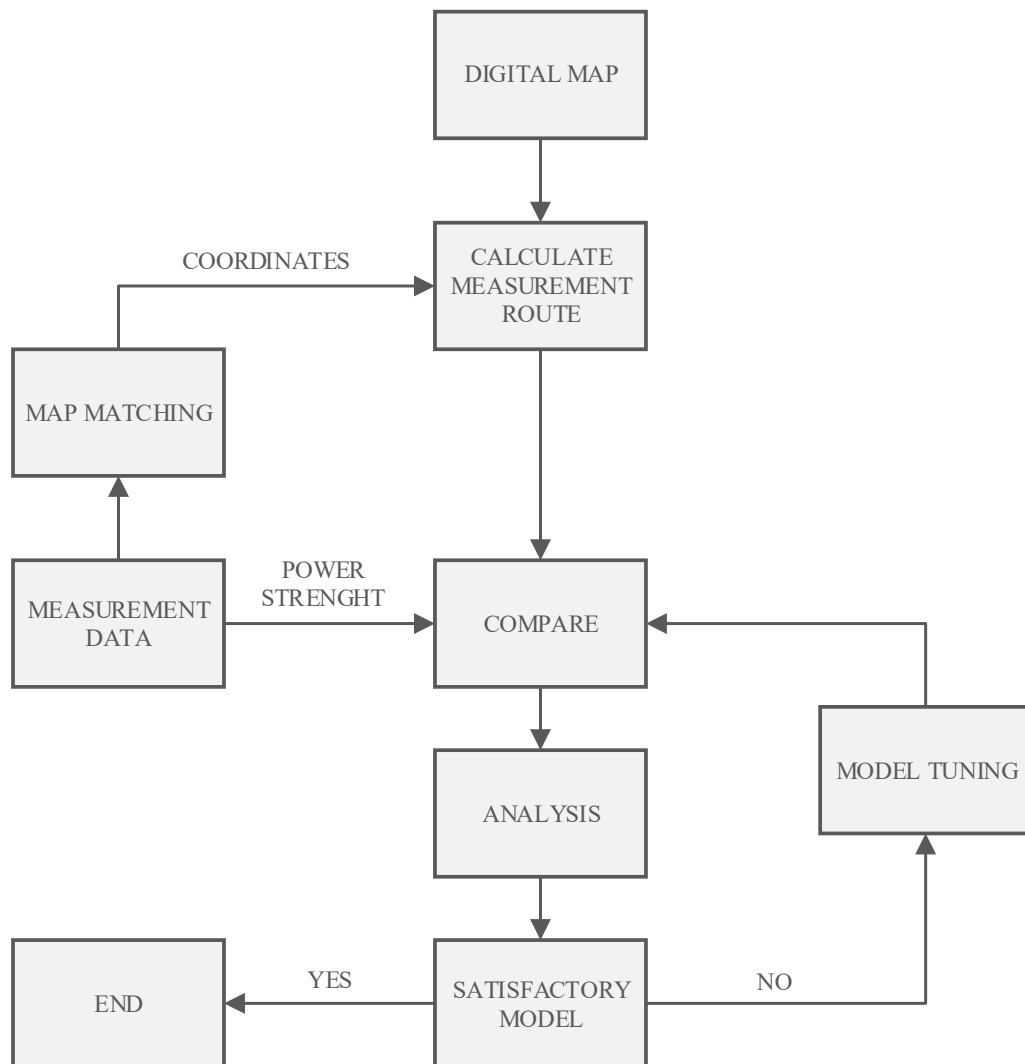


Figure 3.1 Methodology block diagram.

3.1 Equipment

This section describes the equipment used in the measurement setup focusing on the principal characteristics that are important for this project. The devices shown are the ground station antenna LHG 5, the drone antenna SXT Lite5, the router RB951 Ui-2HnD, the Raspberry Pi 3 and GPS module GM-3 N RU300.

3.1.1 Antennas

The ground station uses an antenna of the model LHG 5¹ of the manufacturer Mikrotik. This parabolic antenna provides very high gain with an integrated dual polarization whose physical appearance is shown in Fig. 3.6(a). The operating frequency is within the C band, more precisely with a frequency range from 5150 to 5875 MHz. The main specifications of this antenna are summarized in Table 3.1.

Table 3.1 Specifications of LHG 5 series

Feature	Value
Operating frequency	5150 - 5875 MHz
Maximum antenna gain	24.5 +/- 0.5 dBi
Antenna beam width	7°
Cross polar	15 dBi
Port to port isolation	20 dB
Front to back ratio	25 dB
Return loss	10 dB
Supported input voltage	11 V - 30 V
Operating Temperature	-40 to 70° C
Maximum power consumption	6 W
Wireless 5 GHz standards	802.11a/n

The main feature of this antenna is its high directivity that achieves the main lobe gain of 24.5 dBi. According to the datasheet, the main lobe has a narrow beam width of 7° that will produce considerable loss of gain when the antenna is not properly pointed. The antenna specifications also include information related to the diagram pattern of the two main planes. Fig. 3.2 and 3.3 show the azimuth and elevation plane diagrams respectively. These plots present the gain of the antenna in dBi, with a maximum value in both cases of 24 dBi. To know the beam width of these patterns, two markers have been placed at 3 dB below the maximum point, obtaining beam widths of 5.5° in azimuth and 5° in the elevation.

¹Mikrotik LHG 5 (RBLHG-5nD). <https://mikrotik.com/product/RBLHG-5nD>

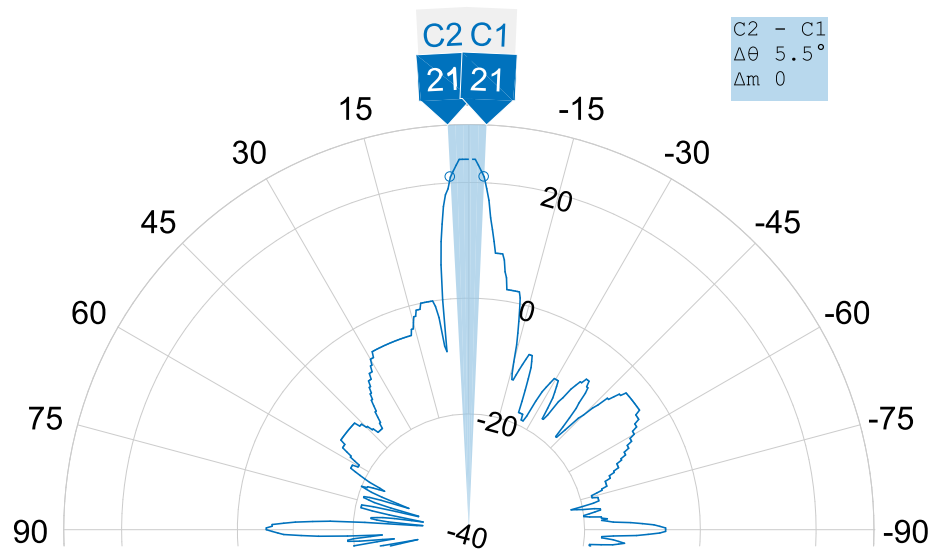


Figure 3.2 Mikrotik LHG 5 azimuth gain pattern.

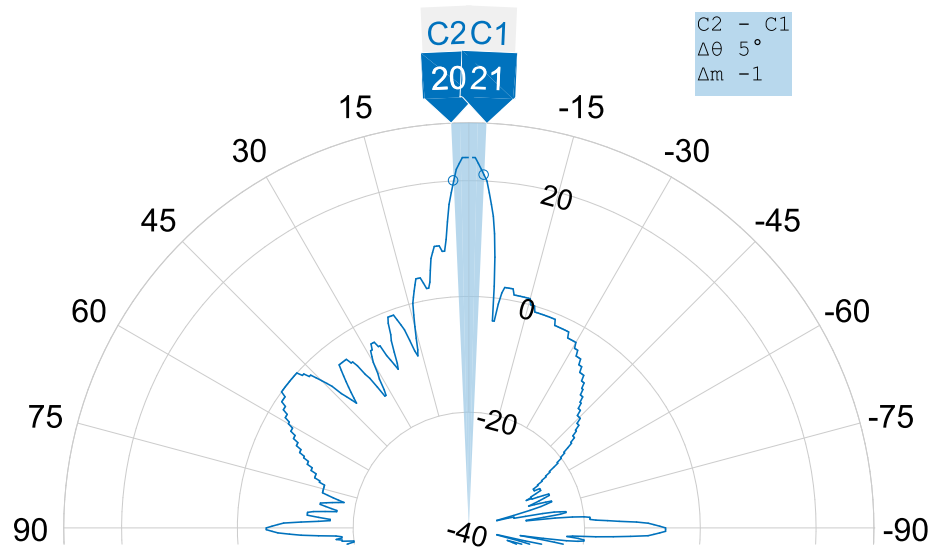


Figure 3.3 Mikrotik LHG 5 elevation gain pattern.

The drone uses the antenna SXT Lite5² of Mikrotik, that works at the C band with a frequency range from 4920 to 5920 MHz. The principal features of this device are collected in the Table 3.2. The SXT Lite5 has a wider beam width compared with the narrow diagram provided by the antenna of the ground station. In this case, the antenna is formed by 9 square patch placed in an array structure of 3x3 as

²Mikrotik SXT Lite5 (RBSXT5nDr2). <https://mikrotik.com/product/RBSXT5nDr2>

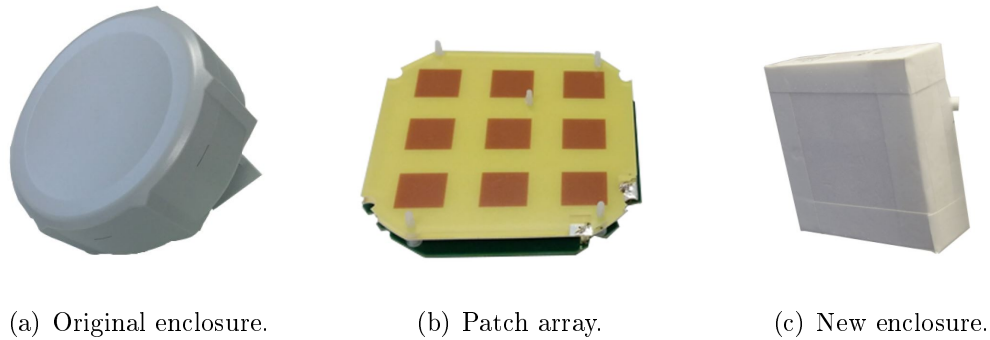


Figure 3.4 Mikrotik SXT Lite5.

Fig. 3.4 shows. Taking into account that this antenna is going to be mounted on the UAV, the problem is its heavy weight. Fortunately, the most heavy part is the weatherproof enclosure that protects the internal array. To improve the performance of the UAV, the external enclosure has been replaced by a lighter material, as it is shown in Fig. 3.4(c).

Table 3.2 Specifications of SXT Lite5

Feature	Value
Operating frequency	4920 - 5920 MHz
Maximum antenna gain	16 dBi
Antenna beam width	25°
Port to port isolation	35 dB
Supported input voltage	8 V - 32 V
Operating Temperature	-30 to 80 °C
Maximum power consumption	7 W
Wireless 5 GHz standards	802.11a/n

Patterns of the drone antenna are not provided by the manufacturer. It is necessary to create them from the antenna parameters. The maximum gain and beam width are taken as reference in order to approximate the gain diagrams. The antenna behaviour has been simulated using a low pass Chebyshev filter. To achieve the right gain and beam width, the window length and the side lobe magnitude need to be optimized. The Fig. 3.5 shows the final gain pattern of the drone antenna that has a maximum value of 16 dBi. The markers C1 and C2 placed 3 dB below the maximum gain, present the antenna beam width of 24.96° close to the specified value of 25°.

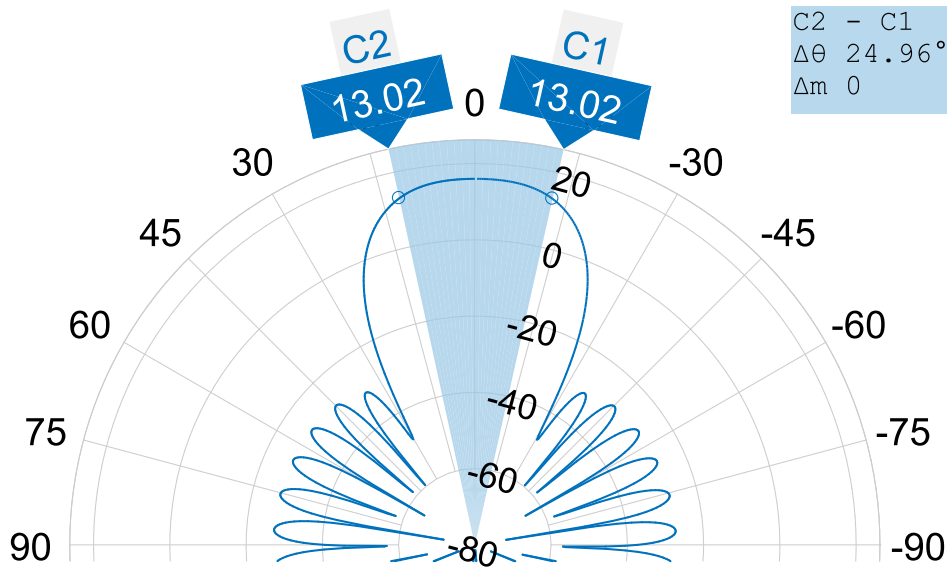


Figure 3.5 Mikrotik SXT Lite5 gain pattern.

3.1.2 Additional hardware

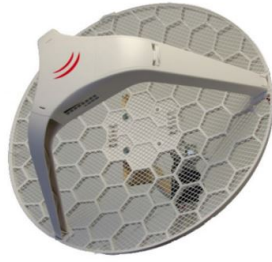
A router is mounted in the UAV in order to provide access to the clients. The chosen device is the Mikrotik RB951Ui-2HnD³ that works in the band of 2.4 GHz. It has five Ethernet ports and one USB 2.0 port as Fig. 3.6(b) shows. The port number 5 has the particularity of providing power, a useful feature which permits to connect external devices. Its main features are presented in Table 3.3.

Table 3.3 Specifications of RB951Ui-2HnD router.

Feature	Value
Operating frequency band	2.4 GHz
Wireless 5 GHz standards	802.11b/g/n
Antennas	2x2 MIMO
Maximum antenna gain	2.5 dBi
Supported input voltage	8 V - 30 V
Maximum power consumption	7 W
Operating Temperature	-20 to 50 °C
Modulations	OFDM: BPSK, QPSK, 16 QAM, 64QAM DSSS: DBPSK, DQPSK, CCK

In the measurement process, one of the antennas is static while the other one is moving to different locations in order to test the link for different distances. To

³Mikrotik RB951Ui-2HnD. <https://mikrotik.com/product/RB951Ui-2HnD>



(a) Mikrotik LHG 5 antenna.



(b) Mikrotik RB951Ui-2HnD router.



(c) Raspberry Pi 3.



(d) GM-3 N RU300.

Figure 3.6 Measurement equipment.

control the antenna that is moving and know its location, an external computer is needed. In this way, a Raspberry Pi 3⁴ device is mounted on this antenna taking into account its small size that will facilitate the measurements process. The main goal of this device is to save the coordinates that are provided by an external GPS module connected to one of its USB ports. An important specification that should be mention is the Raspberry Pi 3 is powered by a 5.1 V. As the required voltage is smaller than the voltage supplied by batteries, this device will need an additional module in order to adapt the power supply. The Fig. 3.6(c) shows the device used in the project.

The GPS module measures the antenna location in order to calculate the distance of the link for every measurement. The chosen GPS device is the GM-3 N RU300 of the brand TSI as Fig. 3.6(d) shows. It consists of an antenna, a back upbattery and a GPS engine that provide superior navigation performance under dynamic conditions in areas with limited sky view.

The principal characteristics of this device are collected in the Table 3.4. We can highlight the high sensitivity up to -165dBm for weak signal operation with-

⁴Raspberry Pi 3. <https://www.raspberrypi.org/products/raspberry-pi-3-model-b/>

out compromising accuracy. This flexible module supports two different satellites constellations, GPS and GLONASS, that can be chosen depending the reception quality. GM-3 N RU300 send, through its serial port, NMEA messages that contain the device coordinates.

Table 3.4 Specifications GM-3 N RU300.

Feature	Value
Sensitivity	-165 dBm
Waterproof factor	IPX7
Antenna	25*25*4mm patch antenna
Supported satellites	GPS and GLONASS
Acquisition time	35 s
Power Consumption	40mA @ 5V / Tracking
NMEA Message	NMEA0183 v3.01, default baud rate 9600
Operating Temperature	-40 to 80 °C
Dynamic	Altitude : 18000m (max.) Velocity : 515m/sec (max.) Acceleration :4G (max.)
Supply Voltage	DC 5V

3.2 Scripts

This section comprises the script development required for the measurement procedure. On the one hand, one of the scripts will be run in the ground station and drone antennas remotely, in order to evaluate the quality received signal. On the other hand, a program will take the coordinates of the measurement locations. With these two sources of information, we are able to analyse the quality signal depending on the antennas' position. Additionally, a third script has been implemented to compute the distance between two coordinates based on the Haversine formula.

3.2.1 Power measurement script

During the measurement process, the main information required to analyse the propagation channel is related to the received signal quality. For the purpose of this project, the antennas will read the received power as well as the Signal to Noise Ratio (SNR). If we fix the transmitted power by one antenna and we obtain the received power in the other one, we will know how the signal has been degraded and consequently how are the channel losses. An additional reading of the SNR can be

taken in order to compare the level of the desired signal to the level of background noise.

$$SNR(dB) = 10 \log_{10} \left(\frac{P_{signal}(mW)}{P_{noise}(mW)} \right) = P_{signal}(dBm) - P_{noise}(dBm) \quad (3.1)$$

This desired information is captured by the antennas, however, it is not stored in any memory of this equipment. Consequently, a script needs to be implemented in order to save this data and analyse it afterward. The Mikrotik equipment provides a scripting language that can be stored in the Script repository or can be written to the console directly.

This Mikrotik scripting language has its own programming rules that are described in the manual [20]. This manual explains all the commands that this scripting language includes such as data types, operators, variables, functions, loops, etc. To understand how the program has been implemented it is necessary to mention that the comments are introduced by the symbol "#". Moreover, every command should start with the ":" token, otherwise it will be treated as a variable. As this measurement script needs to be executed frequently, it will be stored in the Script repository that all the Mikrotik's devices include.

The Appendix A.2 shows the script uploaded in the ground station and drone antennas which reads the desired information and save it in a file. The following description of all the script steps explains how the signal information is taken:

- In the first part of the code, **Option settings**, the principal settings of the power measurement are defined. It sets how many samples are taken with the local variable *testSamples*. In the same way, it defines the time difference between samples with the variable *delaySamples* set in seconds. Moreover, with the definition of the global variable *testNumber*, the script defines the number of the current measurement. By default, the script takes a total of 10 measurements with a time slot of 1 second.
- Then, in the **File creation**, a ".txt" file is generated according to the *testNumber*. Considering a script execution where *testNumber* equals to 1, the file where the measurements are saved is called *range_test_1*.
- Several local variables are defined in the **Variable definition** segment with the purpose of saving the different signal parameters. These parameters are:
 - *signalStrength*. Integer which has the average strength of the client signal received by the antenna.

- *signalToNoise*. String which contains the SNR of the antenna.

Mention that an additional parameter, *BREAK*, has been included in the string variable due to the Mikrotik script language does not include a command for line breaks. In the analysis process, this parameter will be changed by a line break.

- Once the options have been set and the required variables and files created, we need to take the information that the antenna is reading and save it in the right place as the **Measurement process** shows. As this process needs to be repeated as many times as the variable *testSamples* indicates, the program includes a "for" loop that measures the antenna parameters in several iterations.

During each iteration, the received power and the SNR are taken from the *Wireless registration table* and copied in a string variable. The last part of the loop includes a delay command that stops the execution as *delaySamples* indicates.

- In the last part of the code **Data saving**, all the measurement information is copied in the proper file.

At this point, a practical example shows the steps that the operator should follow in order to achieve the measurements properly. All these commands need to be written in the terminal of the ground station and drone antennas.

1. First we need to access to the *system* menu, where the scripts are run.

```
/system
```

2. Define the variable *testNumber* with the desired number. (In this example 1).

```
:global testNumber 1
```

3. Run the following command in order to start the measurements. We should run this command twice. In the first iteration, the script will create a new file and in the second one, it will save the measured values. The word *antennaMeasurement* refers to the name of the script which is saved in the script file of the Mikrotik equipment.

```
/script run antennaMeasurement
```

4. If we want to save new values in a new file, we just have to repeat the second and third steps, setting a different *testNumber*.

```
:global testNumber 2
/system script run antennaMeasurement
```

The following code shows the content of the *range_test_1.txt* file with the default values of 10 samples with a time slot of 1 second.

```
TEST 1 BREAK; id; signalStrength; signalToNoise; BREAK; 1; -32; 69;
BREAK; 2; -32; 72; BREAK; 3; -31; 74; BREAK; 4; -31; 75; BREAK;
5; -32; 75; BREAK; 6; -32; 75; BREAK; 7; -32; 75; BREAK; 8;
-32; 76; BREAK; 9; -32; 76; BREAK; 10; -32; 76; BREAK;
```

After editing this data, the information is shown in a table format as Table 3.5.

Table 3.5 Example of range_test_1.txt.

Measurement	Signal Strength (dBm)	SNR (dB)
1	-32	69
2	-32	72
3	-31	74
4	-31	75
5	-32	75
6	-32	75
7	-32	75
8	-32	76
9	-32	76
10	-32	76

3.2.2 GPS script

To model the propagation loss depending on the distance between antennas, an accurate method to compute the antennas' locations during the measurement process is required. An external GPS module of the model GM-3 N RU300 will take the coordinates of both antennas, enough information to compute the link distance. This device provides NMEA (National Marine Electronics Association) packets that need to be filtered in order to take only the desired information about coordinates. The Python program shown in Appendix A.1 will take the coordinates during the measurement process.

To understand how the program works, it is necessary to explain the main aspects of the NMEA syntax summarized in [4]. Each sentence begins with a '\$' and can be

no longer than 80 characters of visible text. The data is contained within this single line with data items separated by commas. The data itself is just ASCII text and may extend over multiple sentences in certain specialized instances but is normally fully contained in one variable length sentence. The only NMEA sentence that concerns to this program is `$GNRMC`, which provides coordinates according to information of satellites systems GPS (Global Positioning System) and GLONASS (Global Navigation Satellite System). The following sentence shows an example of the `$GNRMC` command that the GM-3 N RU300 device can read.

```
$GNRMC ,220516 ,A ,4916.45 ,N ,12311.12 ,W ,173.8 ,231.8 ,130694 ,004.2 ,W*70
```

The structure of this command is divided into twelve parts that give information about the longitude, latitude and more parameters that are not relevant to this application. The Table 3.6 shows the meaning of each of these parameters.

Table 3.6 Parameters of `GNRMC` command.

	Value	Definition
1	220516	Time Stamp
2	A	Navigation receiver warning A = OK, V = warning
3	6127.184585	Latitude 61 deg. 27.184585 min
4	N	North/South
5	02350.650980	Longitude 23 deg. 50.650980 min
6	W	East/West
7	173.8	Speed in knots
8	231.8	True course
9	130694	Date Stamp
10	004.2	Magnetic variation
11	W	East/West
12	*70	Mandatory checksum

The GPS module is going to be mounted in one of the antennas that is moving through different distances. To run the program shown in Appendix A.1, that reads the coordinates of each location, a Raspberry Pi 3 is needed. In this way, the GPS module is connected to the serial port of the Raspberry which will execute the script remotely. A description of all the script steps explains how the coordinates are read.

- In the first part of the code, we need to import the packages that this Python program requires. As the GPS information is read from the serial port, the `serial` package is needed. As the script will use input arguments, it also imports the `argparse` package.
- To read the NMEA information, a method of the `serial` package is used. We need to set the USB port where the GPS module is connected. In this case, it

is connected to the port *ttUSB0* of the Raspberry. Moreover, the baud rate should be fixed according to the datasheet specification that recommends a rate of 9600.

- In the third part of the program, *Argument definition*, we take the arguments values that are given when the GPS script is executed. The script only has one argument which indicates the *ID* of the measurement.
- Finally, the measurement process uses a *while* loop that runs indefinitely thanks to the true condition. This loop checks all the NMEA sentences until a *\$GNRMC* sentence arrives. Then, the script verifies if the navigation receiver warning has the value A, which indicates that the provided information is correct. In the last part, the script saves the coordinates in the file *position.txt*. It saves in the same line the ID, longitude and latitude of each measurement.

At this point, a practical example shows how the script should be run by the operator that wants to make the coordinates measurements. Mention that this program needs to be executed in a device with Python installed.

1. We need to run the following command, setting the *ID* number in the argument *-i*. In the first measurement, the argument should be 1.

```
python measureGPS.py -i 1
```

The script will return a terminal line with the measured values. The operator can verify if the measurement is made properly. If there is any problem, the same command will read the coordinates again. This is an example of what the program returns.

```
Measurement; 1;Latitude; 6127.184585;Longitude; 02350.650980
```

2. Then, the operator will change the antenna location and execute the same script again. The argument *-i* needs to be increased in every measurement. For instance, during the second position measurement, the command would be

```
python measureGPS.py -i 2
```

3. The coordinates information is saved in a file called *position.txt* that has the following structure after an example of 5 measurements.

```
Measurement; 1;Latitude; 6127.166713;Longitude; 02350.647804
Measurement; 2;Latitude; 6127.171616;Longitude; 02350.623645
```

```

Measurement; 3;Latitude; 6127.168271;Longitude; 02350.619255
Measurement; 4;Latitude; 6127.166667;Longitude; 02350.617561
Measurement; 5;Latitude; 6127.163891;Longitude; 02350.610819

```

It is important to highlight the coordinate format that the NMEA syntax provides as Table 3.6 shows. In the latitude term, the two first digits refer to the degrees while the rest of the digits specify the minutes of the coordinates. The same happens with the longitude measurements. These units are going to be transformed to a unique degree value as the equation 2.45 requires.

3.2.3 Haversine script

Once the GPS script has measured the coordinates information, an additional script needs to be executed to calculate the distance between those distances. The Matlab program shown in Appendix A.3 implements the Haversine equation 2.45 that provides the distance between two locations, given their latitude and longitude in degrees. During the propagation channel measurements, one of the antennas remains in the same position while the operator moves the other antenna and test the channel for different distances. Therefore, this program will have as inputs, the coordinates of the static antenna $lat1$ and $long1$, and a set of locations given as two vectors $lat2$ and $long2$. All these latitude and longitude values should be transformed to radians in order to use the Matlab trigonometric functions.

When the Haversine formula is implemented, the program uses the function $atan2()$ which calculates the arc tangent of the ratio of its two parameters. It is recommended to use this function because it handles the cases automatically when the denominator equals to zero. However, the distance given by the Haversine algorithm needs to be corrected due to the antennas are not placed on the ground. For this reason, a height correction is applied based on the Pythagoras's theorem as Fig. 3.7 shows. The Haversine formula provides the distance between two coordinates d , therefore, the distance is corrected taking into account the height difference between the two antennas obtaining the final distance d' .

A practical example shows the performance of this script considering that the ground station antenna is located at $(61.45412720^\circ N, 23.84418447^\circ E, 20m)$ and the drone antenna at $(61.45391653^\circ N, 23.84341226^\circ E, 2m)$. This example supposes a typical height of the flying UAV of 20 meters and a height of 2 meters for the ground station. With these input values, the Haversine script provides the values of $d = 41.0m$ and $d' = 44.8m$. As it was expected, the distance d' is a bit larger due to it considers

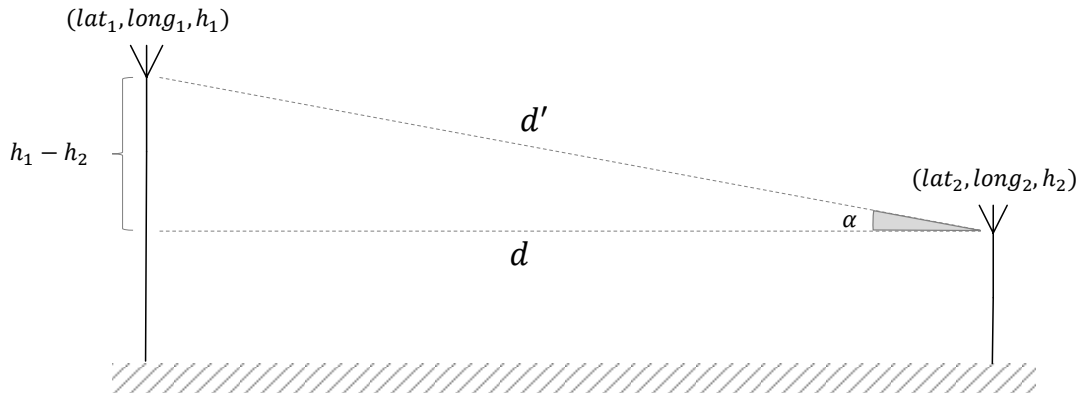


Figure 3.7 Height correction for Haversine algorithm.

the height of both antennas. This method can be verified using a digital map as Google MAPS [3], which provides distances given a set of coordinates. Using this online tool, the distance between the coordinates of this example is 46m. Therefore, this Haversine script is validated.

3.3 System setups and procedures

To measure the propagation channel, many samples need to be taken with different scenarios and distances. If we want to collect enough information about each scenario, the measurement process should be automatized and permit that the operator can easily take all the samples from the same device. This section describes the network setup as well as the steps that the operator should follow to obtain the channel measurements.

3.3.1 Network setup

The network has been configured in order to permit that any device can be reachable from any other device of the same network. In this way, a total of five sub-networks presented in Table 3.7, interconnect all the equipment.

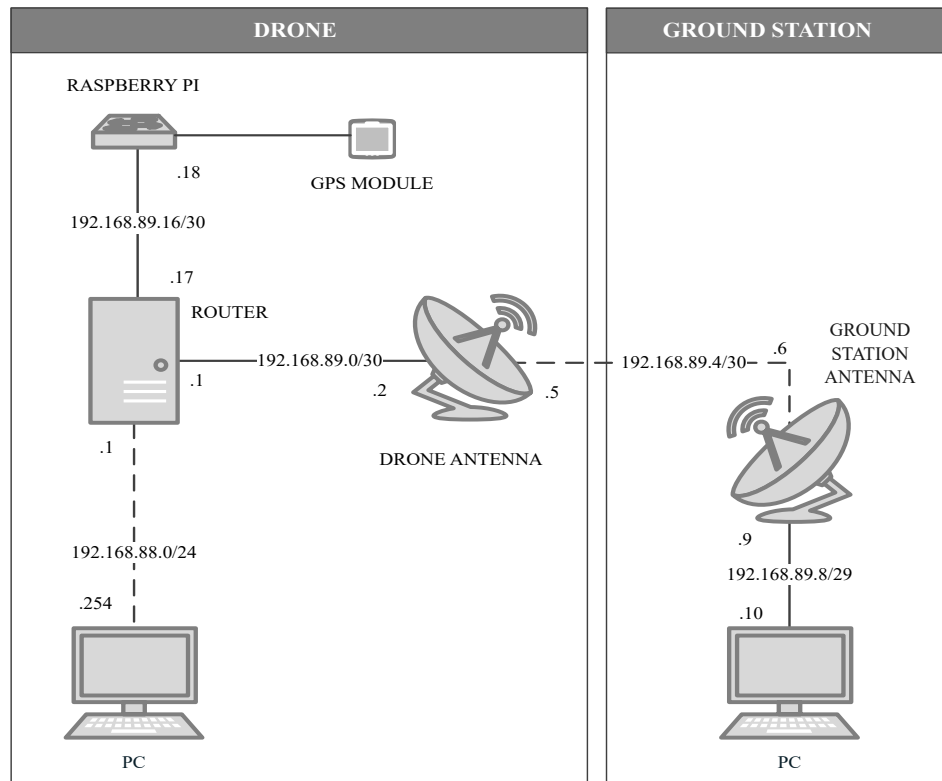
The Fig. 3.8 shows the general configuration of the network that is divided into two main parts, the drone and the ground station blocks. The solid lines show the wire connection between devices, whereas the discontinuous lines present the wireless interfaces. In the drone block, the router acts as a central node connecting the rest of devices. For this purpose, two Ethernet ports of the router connect the UAV antenna and the Raspberry Pi. Mention that the UAV antenna must

Table 3.7 Sub-network IP configuration

Network	Mask	Addresses	Range
192.168.88.0/24	255.255.255.0	253	192.168.88.1-192.168.88.254
192.168.89.0/30	255.255.255.252	2	192.168.89.1-192.168.89.2
192.168.89.4/30	255.255.255.252	2	192.168.89.5-192.168.89.6
192.168.89.8/29	255.255.255.248	4	192.168.89.9-192.168.89.14
192.168.89.18/30	255.255.255.252	2	192.168.89.17-192.168.89.18

be connected to the port 5 of the router, due to this port also provides power. Moreover, the wireless interface of the router allows connection to external devices such as computers and mobile phones. The ground station only needs one sub-network in order to connect the antenna to the backbone link. Furthermore, both antennas are connected through their wireless interfaces.

The network has been designed using the less possible number of IP addresses in each sub-network. Every sub-network has reserved one address that refers to that network, and another address for broadcast. The wireless interface of the router has a total of 253 where the future clients will be connected to. The rest of the sub-networks, as only need to connect two devices, has two available IP addresses.

**Figure 3.8** IP Network configuration.

The Fig. 3.8 presents how the initial network is set. However, depending on the measurement scenario, the devices' position can be changed. For instance, if we need to measure the GPS coordinates of the ground station, the Raspberry Pi and the GPS module can be connected to the sub-network 192.168.89.8/29 to take that information.

During the measurement process, the operator needs to connect his computer to one of the main blocks. The computer can be connected either to the UAV block with the router or to the ground station block with the antenna Ethernet port. In this way, all the scripts can be executed from the same terminal using an SSH client. For this project, the free software PuTTY ⁵ has been used. To verify the network operation, PING commands have been sent to every device from the computers placed in the endpoints of the network, to test if all the devices are reachable.

3.3.2 Measurement setup

According to the network described in the Fig. 3.8, this section explains how the equipment needs to be connected and supplied. The main setup used in this project is shown in the Fig. 3.9. All the equipment is mounted on tripods with a height range from 1.5 to 3.5 meters that allow us to measure the channel with different antenna heights. During the measurements, one of the antennas remains static while the other tests the channel for different locations. The mobile antenna is connected to the GPS module which saves the coordinates of every tested position.

The equipment is supplied with LiPo batteries of four cells which provide an output voltage of 14.8 volts. Each tripod contains one battery that supplies all the equipment mounted on it. It is important to summarize the supported voltage by each device in order to connect properly each battery. The voltage specifications are shown in Table 3.8.

Table 3.8 Supported voltage of each device.

Device	Voltage range (V)
Mikrotik LHG 5 (Ground station)	11 - 30
Mikrotik SXT Lite5 (Drone)	8 - 32
RB951Ui-2HnD router	8 - 30
Raspberry Pi	4.75 - 5.25
GPS module	5

⁵PuTTY. <https://www.putty.org/>

On the one hand, the battery placed on the drone tripod supplies its entire voltage to the router. As it was mentioned before, the drone antenna uses a specific Ethernet port of the router, which also provides 14.8 V as this antenna requires. On the other hand, the ground station block demands a voltage regulator in order to adapt the battery output from 14.8 V to 5 V, to supply the Raspberry Pi. The GPS module is connected to the Raspberry Pi 3 with the USB port which also provides the required voltage of 5 V.

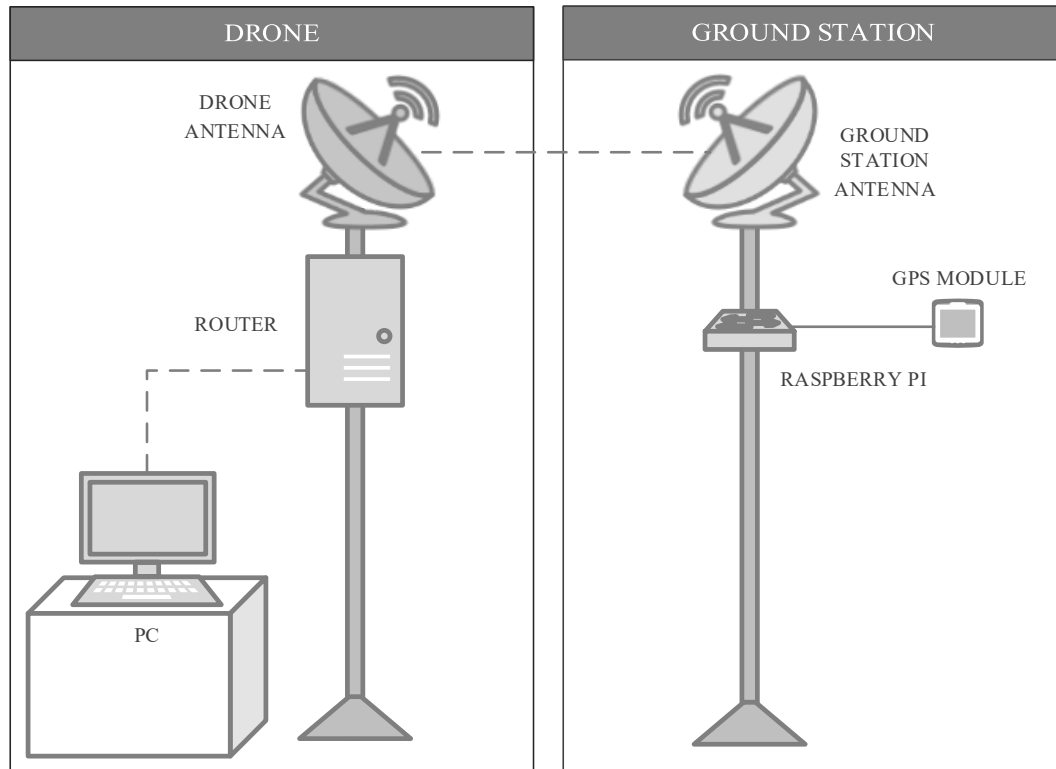


Figure 3.9 Measurement setup.

The Fig. 3.10 shows the battery connections in the drone and ground station blocks. The different supported voltages, 5 and 14.8 V, are presented in red and blue, respectively. The most significant part of this supply configuration is the voltage regulator which needs to be tuned in order to properly transform the output voltage of the battery. The commercial component used for this block is the LM2575⁶ switching regulator, which provides a fixed output voltage of 5 V.

⁶LM2575 datasheet. <https://www.onsemi.com/pub/Collateral/LM2575-D.PDF>

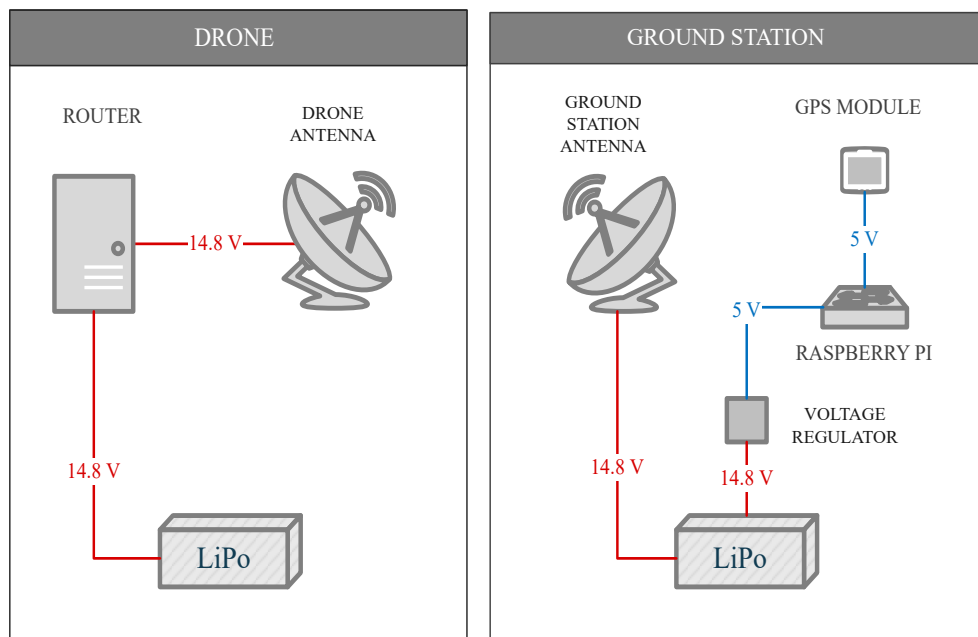


Figure 3.10 Battery configuration.

3.3.3 Measurement procedure

Once the hardware and software involved in the system have been explained, it is important to describe the required steps that must be followed during the measurement procedure. The used setup is comprised of two main blocks shown in Section 3.3.2, the drone and the ground station blocks.

For these measurements at least two people are needed. One person should be focused on running the proper scripts while the other one is moving the transmitting antenna through different locations. The person who executes the scripts is going to be placed next to the drone antenna which will remain static at the same location. This person will connect his PC to the network presented in Fig. 3.9 through the wireless interface of the router. As every device of the network is reachable as it was explained in Fig. 3.8, the operator will connect his PC to the drone antenna and to the Raspberry. Using an SSH session, both devices are controlled remotely.

The following steps should be repeated at different locations to measure the channel response depending on the distance:

1. Connect a PC to the router with the Wi-Fi interface and open two terminals

using SSH session in the drone antenna and the Raspberry Pi. The drone bock acts as a receiving antenna.

2. The ground station block, which includes the GPS module, will be placed firstly at the same location of the drone block. Using the *GPS script* described in Section 3.2.2 the coordinates of the drone antenna are taken. This location is considered as reference in order to compute the link distance.
3. The second operator will move the ground station block to the first location. Then, the operator that is connected to the PC, will run two scripts at the same time. On the one hand, the *GPS script* reads the coordinates of that position in order to compute the link distance according to the *Haversine script*. On the other hand, the *Power measurement script* saves the receiving power by the drone antenna.

Repeating this procedure at different locations, we are able to analyse how the signal is degraded depending on the distance between the transmitting and the receiving antennas. This is the principal information needed to implement an empirical propagation model.

4. MEASUREMENT ANALYSIS

The measurement campaign was performed in Hervanta, Finland. The environment is a suburban medium size city where the antennas are placed in locations with LOS, surrounded by buildings with an average height of 12-15 m (4-5 floors). The antennas have been tested along streets of 30 m width without any obstacle, as the environment where the system will be deployed in the future. To model the propagation loss of the link, three alternative scenarios have been analysed considering different antenna heights.

4.1 Measurement locations and procedures

During the operation of the real system, the ground station will provide a ground connection to the UAV that will fly at heights up to 30 meters. To simulate the behaviour of the system at such heights, three different scenarios have been measured varying the UAV antenna height from 7 to 27 meters. The Table 4.1 summarizes the main characteristics of the scenarios that this project will analyse. This table shows the height used in every measurement as well as its distance range. Moreover, the coordinates of the two main locations of the measurement process are shown, indicating their latitude and longitude as ϕ and λ , respectively. The location X refers to the position where the UAV antenna has been placed. The location Y indicates the final position where the ground station antenna has been tested. The Fig. 4.1 shows the routes used during the measuring campaign in the three different scenarios specifying the locations X and Y mentioned before.

Table 4.1 Summary of the measurement scenarios.

	Height	Range	Locations	Location X	Location Y
A	$h_A = 7m$	30-560 m	31	$\phi_X = 61.4528137^\circ N$ $\lambda_X = 23.8446471^\circ E$	$\phi_Y = 61.4506615^\circ N$ $\lambda_Y = 23.8351349^\circ E$
B	$h_B = 9.5m$	30-520 m	35	$\phi_X = 61.4530764^\circ N$ $\lambda_X = 23.8441830^\circ E$	$\phi_Y = 61.4508049^\circ N$ $\lambda_Y = 23.8356655^\circ E$
C	$h_C = 27m$	50-240 m	19	$\phi_X = 61.4541272^\circ N$ $\lambda_X = 23.8441844^\circ E$	$\phi_Y = 61.4529663^\circ N$ $\lambda_Y = 23.8404807^\circ E$

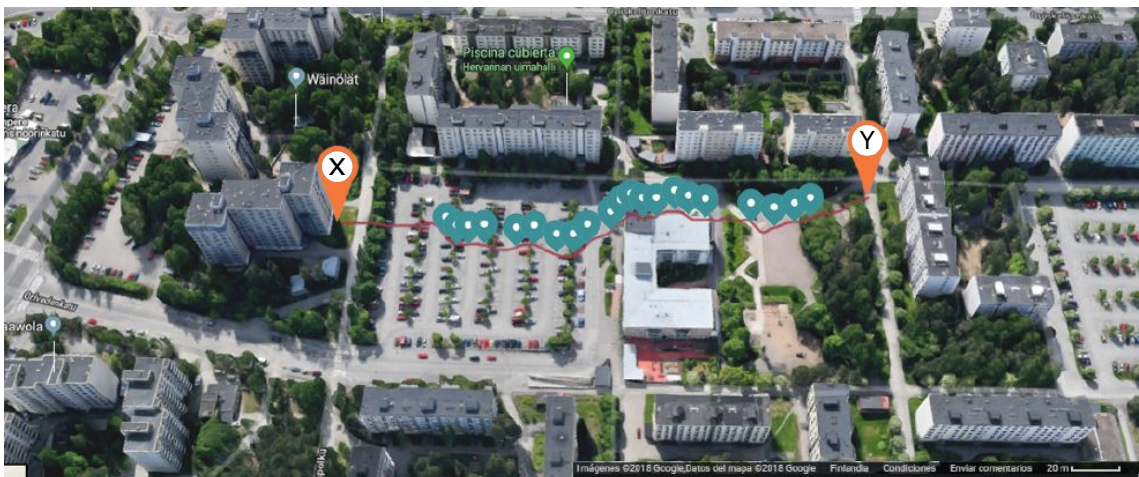
(a) Measurement locations in scenario A with $h_A = 7m$.(b) Measurement locations in scenario B with $h_B = 9.5m$.(c) Measurement locations in scenario C with $h_C = 27m$.

Figure 4.1 Measurements routes. The figures are extracted from Google Maps [3] with its permission

As the Fig. 4.1 shows, several measurements have been taken in each scenario using the setup introduced in Section 3.3.2. The equipment used in these measurements is shown in Fig. 4.2, which is the real implementation of the theoretical setup described in Fig. 3.9. The scripts explained in Section 3.2 have been set in order to take a total of 10 samples with a time slot of 1 second per location.

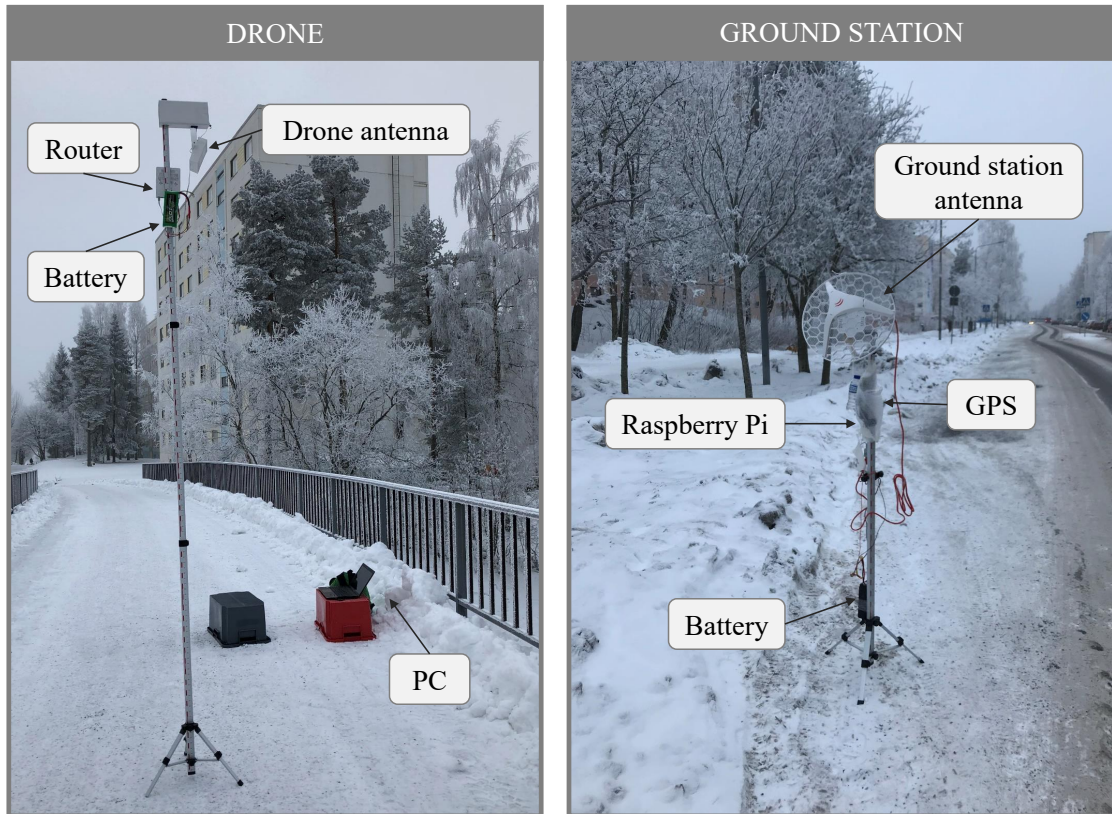


Figure 4.2 Real setup used during channel measurements.

In this way, the scenario with the drone antenna with a height of $h_A = 7m$ has been tested along 31 locations moving the ground station from distances between 30-560 m compared with the static antenna. The second scenario which places the drone antenna at $h_B = 9.5m$, analyses the channel for distances between 30-520 m along 35 locations. Finally, the third scenario allocates the drone antenna at a very tall location of $h_C = 27m$, taking into account a total of 19 ground station positions with distances up to 240 m.

The Fig. 4.3 shows the environments where the measurement campaign took place. On the one hand, the scenarios A and B were performed in a long street that has a bridge of 6 meters, as the pictures 4.3(a) and 4.3(b) present. The tripod where the drone antenna is mounted, allows varying the height of this antenna in order to obtain the total height of 7 and 9.5 meters explained before. On the other hand,



(a) Drone antenna location in scenarios A and B. (b) LOS locations in scenarios A and B.



(c) Drone antenna location in scenario C. (d) LOS locations in scenario C.

Figure 4.3 Scenario environments.

in the scenario C, the drone antenna was placed on the ninth floor (27 m) of the building as the pictures 4.3(c) and 4.3(d) show.

4.2 Elevation profile

According to the coordinates measured in the three different scenarios, the elevation profile of each environment will be analysed in order to verify if there were not any obstacles that could corrupt the measurements. The height information has been taken using the online tool Geocontext [2], that provides elevation profiles in CSV files. This tool permits to import coordinates files in GPX format. An additional website, GCPX [1], has been used in order to generate the GPX files that will be uploaded to Geocontext.

Once we have the elevation profile of each scenario, we can do a preliminary analysis about how the environment interferes to the signal taking into account the Fresnel concepts explained in Section 2.1. Just as a recap, the main part of the signal energy is transmitted in the first Fresnel zone. This zone is an ellipsoid volume whose radius is approached with the following expression:

$$R_1 = 548 \sqrt{\frac{d_1 d_2}{(d_1 + d_2) f}} \quad (4.1)$$

A new concept is introduced to specify with more accuracy the drone antenna height in each scenario. This concept is the effective height of the antenna, h_{eff} , that indicates the elevation of the antenna compared to the average terrain height. For every scenario, the first Fresnel zone and effective height concepts are studied below. Mention that the frequency used in these measurements was 5580 MHz.

- **Scenario A.** In this scenario, the drone antenna was mounted on a tripod of 1 m placed on top of a bridge of 6 m high. Then, the antenna height over the ground level is $h_A = 7m$. Moreover, the average terrain height has been computed taking a value of 150.8 meters over the sea level, which implies a drone antenna effective height of $h_{eff,A} = 7m$. The elevation profile and the first Fresnel zone of this scenario are shown in Fig. 4.4. As the first Fresnel zone is free of any obstacle, the signal will be propagated without significant losses.

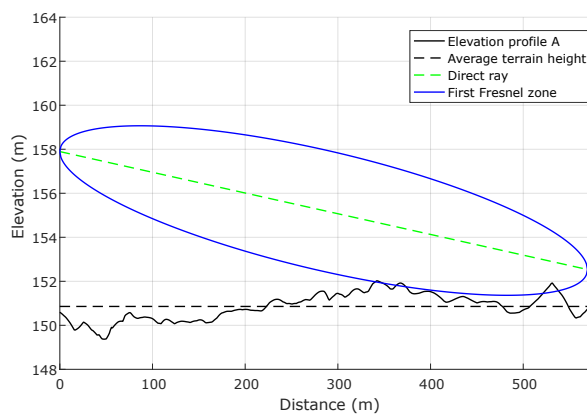


Figure 4.4 Elevation profile and first Fresnel zone at scenario A.

- **Scenario B.** In the second scenario, the drone antenna was placed on the bridge of the scenario A, but in this case, with a longer tripod of 3.5 m. Therefore, the antenna height over the ground level is $h_B = 9.5m$. In this

case, the average terrain height has been computed taking a value of 151 meters over the sea level, giving an effective height of $h_{eff,B} = 11.2m$. The elevation profile and the first Fresnel zone of this scenario are shown in Fig. 4.5. As it was expected, this scenario with a higher antenna height also has the first Fresnel zone free of obstacles.

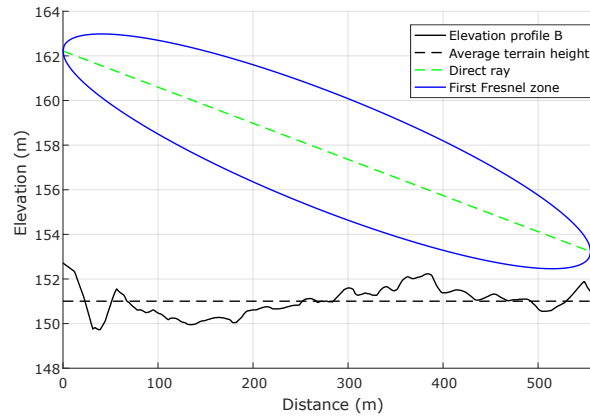


Figure 4.5 Elevation profile and first Fresnel zone at scenario B.

- **Scenario C.** The third scenario considered a higher height placing the drone antenna on the ninth floor of a building, $h_C = 27m$. In this case, the average terrain height was 153.5 m over the sea level, providing an effective antenna height of $h_{eff,C} = 32.6m$. During these measurements, the antennas were placed at LOS locations providing a free first Fresnel zone which allows a good signal propagation. The elevation profile and the Fresnel zone of this scenario are presented in Fig. 4.6.

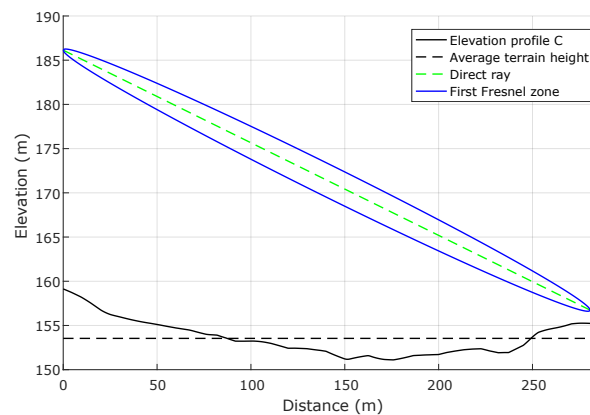


Figure 4.6 Elevation profile and first Fresnel zone at scenario C.

4.3 Calibration

This section explains how the path loss (PL) is obtained and shows how the equipment has been configured in order to measure the propagation channel. The path loss can be calculated with a link budget equation as it was explained in the Section 2.1. This equation relates the power transmitted (P_{TX}) in dBm measured at the TX antenna input port, with the received power (P_{RX}) in the RX antenna output port. This equation considers both transmitter and receiver antenna gains, G_{TX} and G_{RX} respectively in dBi and the path loss PL in dB. In this way, these terms are related as:

$$P_{RX} = P_{TX} - PL(dB) + G_{TX} + G_{RX} \quad (4.2)$$

Then, the path loss can be expressed as follows:

$$PL(dB) = P_{TX} - P_{RX} + G_{TX} + G_{RX} \quad (4.3)$$

During the measurement campaign, the ground station antenna has been set as transmitting antenna, as well as the drone antenna has considered as the receiver. Even in the Section 3.1, several properties of these antennas were presented, the Table 4.2 summarized the principal characteristics that concern to the measurement calibration. The transmitting power by the TX was fixed to 20 dBm using the frequency channel of 5580 MHz. During the analysis of the path loss, the maximum gain of both antennas has been considered, 24 dBi for the transmitting antenna and 16 dBi for the receiving one.

Table 4.2 Summary of the calibrated parameters.

P_{TX}	20	dBm
G_{TX}	24	dBi
G_{RX}	16	dBi
Frequency	5580	MHz

In this way, the signal strength in the receiver side will be collected using the script shown in 3.2.2. As all the terms of the link budget are known excluding the path loss PL , we can easily compute the value of that losses according to the equation 4.3.

4.4 Measurement results

This section shows three sets of measurements made with the same equipment and parameters, only varying the effective height of the receiving antenna. Following the

steps presented in the Section 3.3.3, we are able to relate the measured receiving power with the geographic coordinates where each measurement has been made. As the drone antenna remains fixed during the whole process, we can calculate the distance of each measurement according to the script explained in the Section 3.2.3 based on the Hervasine formula.

The Fig. 4.7 comprises the main results obtained during the measurements, which are going to be used to compute the path losses. This figure describes the received power P_{RX} in dBm, compared to the distance d , expressed in meters. The received power samples describe a linear trend when is compared with the distance in logarithmic units. Each plot of this figure describes the received power according to the effective height of the drone antenna. It can be clearly seen how the P_{RX} decreases when the h_{eff} is higher, obtaining the highest power values for the scenario with a $h_{eff} = 7m$.

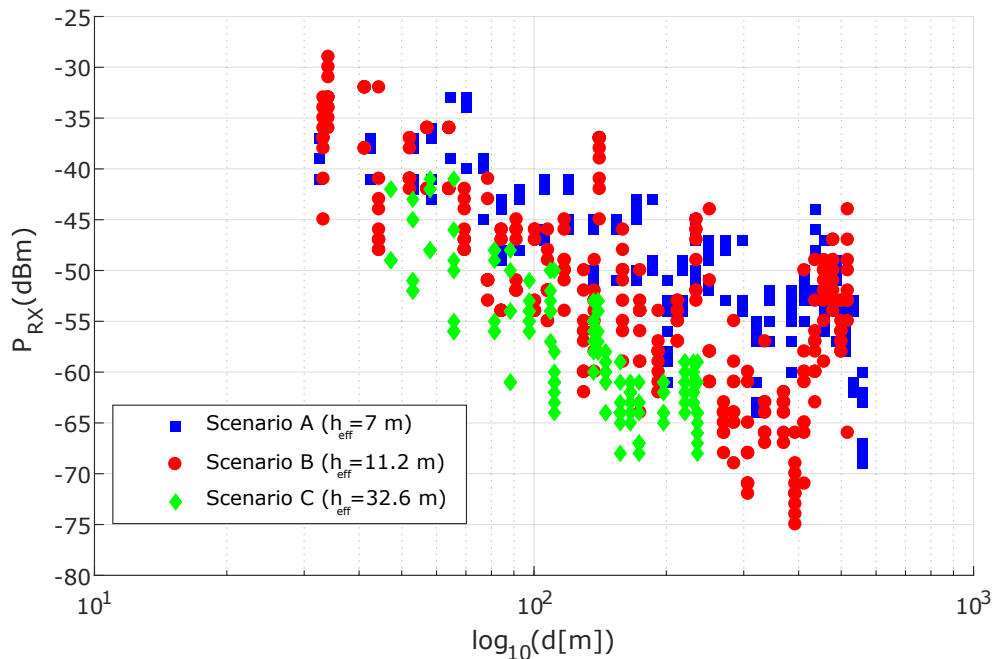


Figure 4.7 Received power samples at scenarios A, B and C.

Once the received power values have been obtained, we can compute the path loss of each channel according to the expression 4.3, taking into account the values shown in the Table 4.2 for the parameters P_{TX} , G_{TX} and G_{RX} . The resulting path loss is presented in the Fig. 4.8, showing the performance of each scenario. As it was expected, the path loss describes a linear trend but with a reverse slope compared to the received power samples. In this case, the channel provides more losses as higher the effective height is, obtaining the worst scenario when $h_{eff} = 32.6m$.

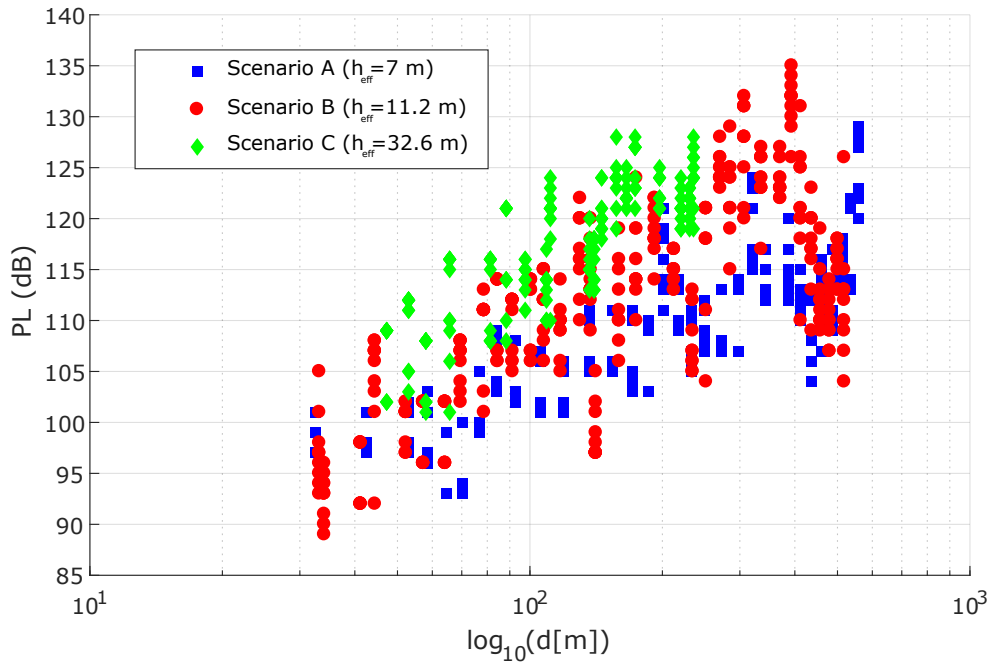


Figure 4.8 Path loss samples at scenarios A, B and C.

4.5 Propagation models comparison

This section shows a comparison between the empirical results obtained during the measurement campaign and some propagation models. In the Section 2.1 several proposals were presented taking into account the formulas and limitations of each model. Therefore, four models that fulfil the characteristics of the studied scenarios are analysed.

- **Free space model.** This approach determines the ideal propagation between the transmitting and the receiving antennas. This model known as FS is described by the equation 2.7.
- **2-ray model.** This model considers the effect when the transmitted signal is reflected in the flat surface where the antennas are placed according to the equation 2.8.
- **SUI model.** This empirical model is designed for frequencies up to 11 GHz and includes corrections depending on the carrier frequency and the base station height as the equation 2.15 shows.
- **Empirical path loss model at 5.4 GHz by Hang Zheng.** This approach intended for the new mobile generation 5G proposes a path loss model summarized in the equation 2.21.

In the first scenario the drone antenna, considered as the base station in some of the studied models, was placed on top of a bridge with an effective height of $h_{eff,A} = 7m$. The transmitting ground station antenna was mounted on a tripod of 1.8 m. Taking into account a carrier frequency of 5580 MHz, the four propagation models have been implemented obtaining the Fig. 4.9. The FS model is the most optimistic, considering the lowest path loss. The 2-ray model shows periodic loss maximums that refer to the destructive contributions of the reflected ray. Conversely, the constructive contributions produce minimums in the path loss a bit lower than the FS model. For this scenario, the SUI model provides the highest path loss.

The same procedure has been applied to the scenario B, taking into account an effective height of $h_{eff,B} = 11.2m$. As the scenarios are very similar, the proposed models present a similar performance as can be seen in Fig. 4.9. As it was expected, the constructive and destructive contributions of the 2-ray model are placed at different distances as the antenna height has changed. The rest of the models do not considerably change compared to the scenario A.

A third analysis has been done with the measurements of the scenario C. Mention that this scenario considers a shorter distance range up to 250 m. The Fig. 4.9 shows the performance of each propagation model when an effective height of $h_{eff,B} = 32.6m$ is applied. The FS model and the empirical path loss model at 5.4 GHz provide a similar response as in the previous scenarios. However, at lower distances, the 2-ray model fluctuates more frequently producing maximums with lower values. As higher the effective antenna height is, the scenario presents more ideal features that can be approximated by the FS model. For this reason, the performance of the SUI model presents a performance more similar to the FS model.

With the analysis of the three scenarios is observed that path loss of this system presents a similar trend than the FS model. The slope of the empirical results describes the same behaviour than the FS model, with the difference of an incremental offset. This higher loss than the measurements presented is originated due to the suburban scenario where the campaign was made. The imperfection of the terrain produces this increase in the path loss.

We can conclude that none of the studied propagation models approach properly the path loss of the environment where this system is going to be deployed. For this reason, we have decided to implement a new propagation model specifically for this system's scenario. In this way, the new propagation model will be more suitable for a system which uses a frequency in the band of 5 GHz and one of its antennas is placed on high heights.

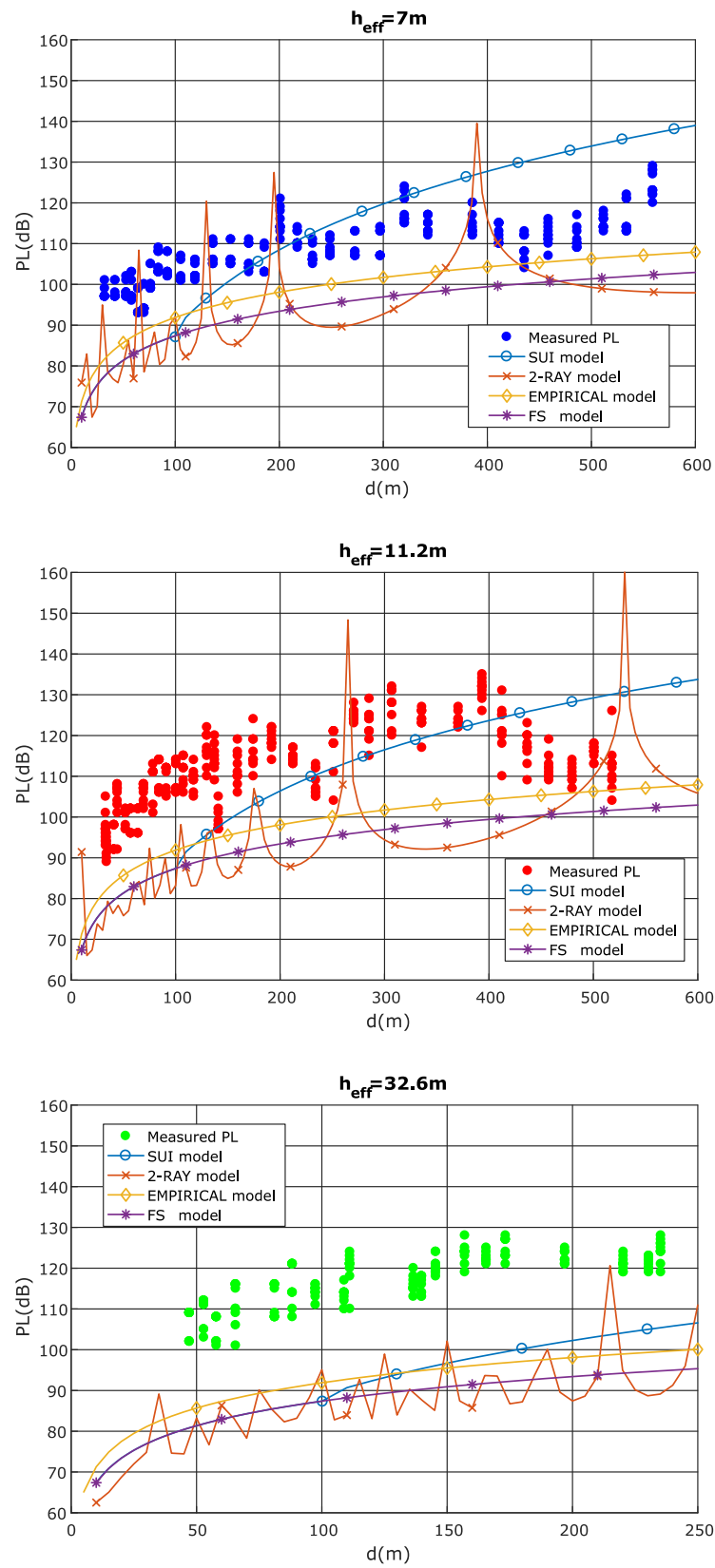


Figure 4.9 Propagation models comparison with empirical results.

5. PROPAGATION MODELLING

This chapter describes the propagation modelling process based on the measurements shown in the Chapter 4, according to the Least Squares method explained in the Section 2.2. The model approach takes as reference measurements made in three different scenarios, obtaining a general expression that describes the path loss depending on the antenna height and the link distance. Moreover, some verifications present the accuracy of the performed model.

5.1 Linear regression approach

Considering the measurements made for the three different scenarios, $i = 1, 2, 3$, we are going to obtain their regression approach applying the Least Squares method. The first linear approximation will relate the path loss with the link distance. As the path losses (L) are represented in logarithmic units, the term that considers the distance (d), will be also represented using logarithms ($\log_{10}(d)$) as this expression shows

$$L_i(dB) = M_i \log_{10}(d) + N_i. \quad (5.1)$$

Using the LS method, the path loss is going to be related to the link distance d in meters, according to two main variables M_i and N_i . The term M_i refers to the path loss slope and is measured in dB/dec. In addition, the constant N_i indicates the intercept point in dB. To obtain the optimum values of the linear regression of each set of measurements, it is necessary to formulate the equation 5.1 as an LS problem with the expression

$$Ax =_{LS} b. \quad (5.2)$$

Considering a particular scenario i , that has been tested at N different distances $d_{i,k}$ with $k = 1, \dots, N$, the vector that contains the path loss for each distance $L_{i,k}$ has been measured. The goal of the LS method is to obtain the optimum solution expressed by the vector

$$x_{LS} = \begin{bmatrix} M_i & N_i \end{bmatrix}^T. \quad (5.3)$$

The vector b refers to the measured values that we want to approach using the LS method. Therefore, this vector includes the path loss measurements $L_{i,k}$ as

$$b = \begin{bmatrix} L_{i,1} \\ L_{i,2} \\ \vdots \\ L_{i,N} \end{bmatrix}. \quad (5.4)$$

The matrix A combines the input values $d_{i,k}$ with the observations $L_{i,k}$, taking into account their relationship with the terms M_i and N_i .

$$A = \begin{bmatrix} \log_{10}(d_{i,1}) & 1 \\ \log_{10}(d_{i,2}) & 1 \\ \vdots & \vdots \\ \log_{10}(d_{i,N}) & 1 \end{bmatrix}. \quad (5.5)$$

The final estimation problem can be formulated as

$$\begin{bmatrix} \log_{10}(d_{i,1}) & 1 \\ \log_{10}(d_{i,2}) & 1 \\ \vdots & \vdots \\ \log_{10}(d_{i,N}) & 1 \end{bmatrix} \begin{bmatrix} M_i \\ N_i \end{bmatrix} =_{LS} \begin{bmatrix} L_{i,1} \\ L_{i,2} \\ \vdots \\ L_{i,N} \end{bmatrix}. \quad (5.6)$$

Notice that according to this matrix notation, every element of the vector b can be expressed as

$$L_{i,k} = M_i \log_{10}(d_{i,k}) + N_i \quad (5.7)$$

with $i = 1, 2, 3$ and $k = 1, \dots, N$, which respects the formulation given by the equation 5.1. Once the LS problem has been properly formulated, it can be solved with the expression explained in the Section 2.2 that concludes with the following LS solution,

$$x_{LS} = (A^T A)^{-1} A^T b. \quad (5.8)$$

Applying this estimation method to the set of measurements of each scenario, we can compute the optimum linear regression line that approaches their path loss. The Table 5.1 presents the main LS results, the slope M_i and the intercept point N_i , of the three scenarios considered for this propagation model. This table clearly shows a trend in the path loss behaviour taking into account the effective height of the receiving antenna. The path loss slope M_i , takes higher values when the antenna height is higher. For instance, the slope in the scenario A with an effective height of 7m has a value of $M_1 = 17.8dB/dec$. By comparison, the scenario C whose effective

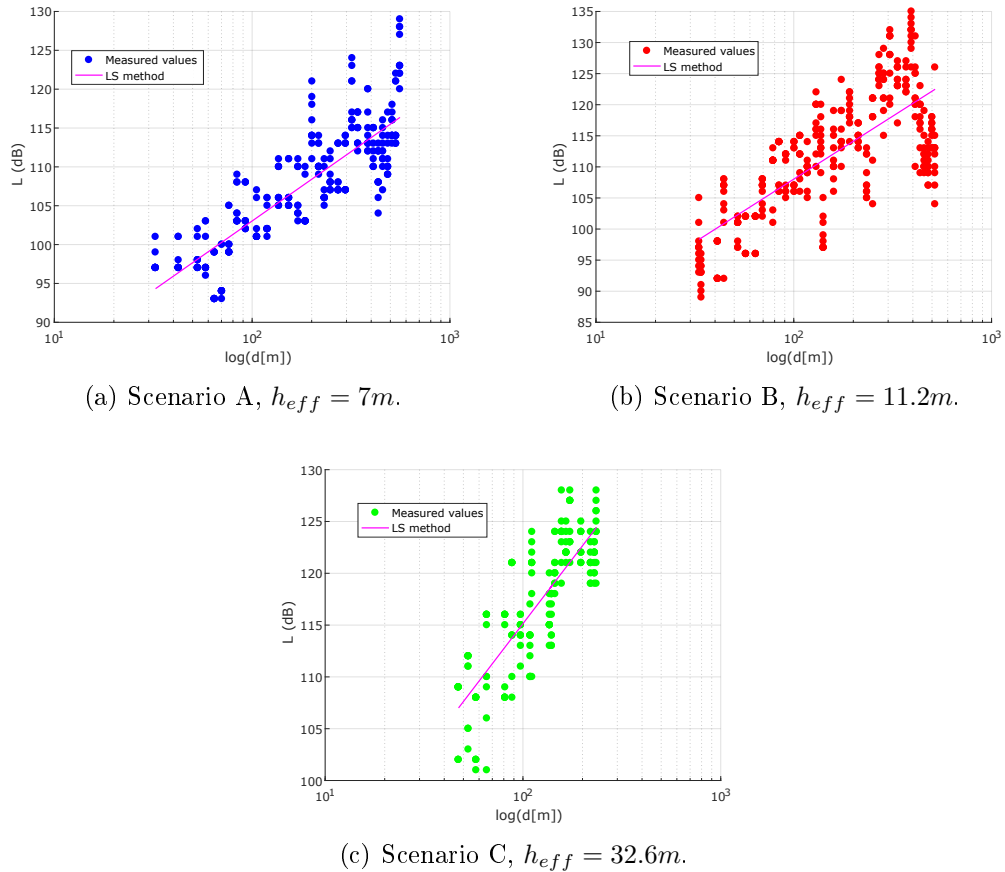


Figure 5.1 Least Squares approach at different scenarios.

height is 32.6m provides a sharper slope of $M_3 = 25.0dB/dec$. The LS results have been implemented and compared with the empirical measurements made in each scenario as the Fig. 5.1 shows.

Table 5.1 Slope and intercept point for LS method

i	Scenario	h_{eff} [m]	M_i [dB/dec]	N_i [dB]
1	A	7	17.8	67.4
2	B	11.2	20.2	67.5
3	C	32.6	25.0	65.2

With the analysis of these path loss results, it can be seen an important dependency on the antenna height. In future sections, the path loss is going to be corrected according to a factor related to the effective height of the antenna.

5.2 Effective height correction

The previous Section 5.1 introduced the linear regression approaches for three different scenarios which consider different effective antenna heights. The objective now is to implement a correction factor that estimates how the path loss changes depending on the height of the antenna. In the Chapter 2, several propagation models were described in order to show different ways to consider the antenna height within those models. The model that has been taken as reference is the Hata model whose path loss is described as

$$L_{Hata}(dB) = 69.55 + 26.16 \log_{10}(f) - 13.82 \log_{10}(h_B) - C_h + [44.9 - 6.55 \log_{10}(h_b)] \log_{10}(d) \quad (5.9)$$

This model corrects the propagation slope with a term that depends on the height of the ground station that multiplies to the distance parameter given by

$$SL_{Hata} = 44.9 - 6.55 \log_{10}(h_b). \quad (5.10)$$

Actually, the slope of this model is described by a linear approach whose main parameter is the antenna height. In a similar way, the intercept point of this model is also represented by a linear approach that depends on the carrier frequency and the ground station height.

$$IP_{Hata} = 69.55 + 26.16 \log_{10}(f) - 13.82 \log_{10}(h_B) - C_h \quad (5.11)$$

Therefore, the idea of this section is to obtain two correction factors for the slope M_i and the intercept point N_i presented in the Section 5.1. For this purpose, the LS method is going to be applied independently to these two parameters as is laid down below.

5.2.1 Slope correction

The slope term described in the expression 5.1 will be formulated as a linear regression taking into account the values M_i with $i = 1, 2, 3$, presented in the Table 5.1. Thus, the new slope is estimated with the following expression,

$$M_i = p + q \log_{10}(h_{eff,i}), \quad (5.12)$$

which depends on the effective height of drone antenna in meters. Repeating a similar process as it was explained in the Section 5.1, we can formulate an LS

estimation problem to calculate the new parameters p and q . The LS problem can be written as:

$$\begin{bmatrix} 1 & \log_{10}(h_{eff,1}) \\ 1 & \log_{10}(h_{eff,2}) \\ 1 & \log_{10}(h_{eff,3}) \end{bmatrix} \begin{bmatrix} p \\ q \end{bmatrix} =_{LS} \begin{bmatrix} M_1 \\ M_2 \\ M_3 \end{bmatrix}. \quad (5.13)$$

Solving this LS problem according to the expression 5.8, we obtain the following parameters:

$$\begin{bmatrix} p \\ q \end{bmatrix} = \begin{bmatrix} 9.0 \\ 10.6 \end{bmatrix}. \quad (5.14)$$

The Fig. 5.2 shows how the slope and intercept values, taken from the measurements of the three scenarios, have been approximated. The left vertical axis of this figure represents the three slope values, M_i , that have been approached with a linear regression described by the parameters p and q .

5.2.2 Intercept point correction

The same process is repeated with the intercept point in order to estimate a linear regression using the values of the Table 5.1 as a reference. In this case, we want to approach the term N_i with two parameters k and l as

$$N_i = k + l \log_{10}(h_{eff,i}). \quad (5.15)$$

An equivalent LS problem is proposed in order to obtain the new parameters. This LS estimation can be formulated as:

$$\begin{bmatrix} 1 & \log_{10}(h_{eff,1}) \\ 1 & \log_{10}(h_{eff,2}) \\ 1 & \log_{10}(h_{eff,3}) \end{bmatrix} \begin{bmatrix} k \\ l \end{bmatrix} =_{LS} \begin{bmatrix} N_1 \\ N_2 \\ N_3 \end{bmatrix}. \quad (5.16)$$

This LS estimation provides the following solution

$$\begin{bmatrix} k \\ l \end{bmatrix} = \begin{bmatrix} 70.7 \\ -3.6 \end{bmatrix}. \quad (5.17)$$

The Fig. 5.2 also represents, with its right vertical axis, how the intercept points N_i have been approached with a linear regression of parameters k and l .

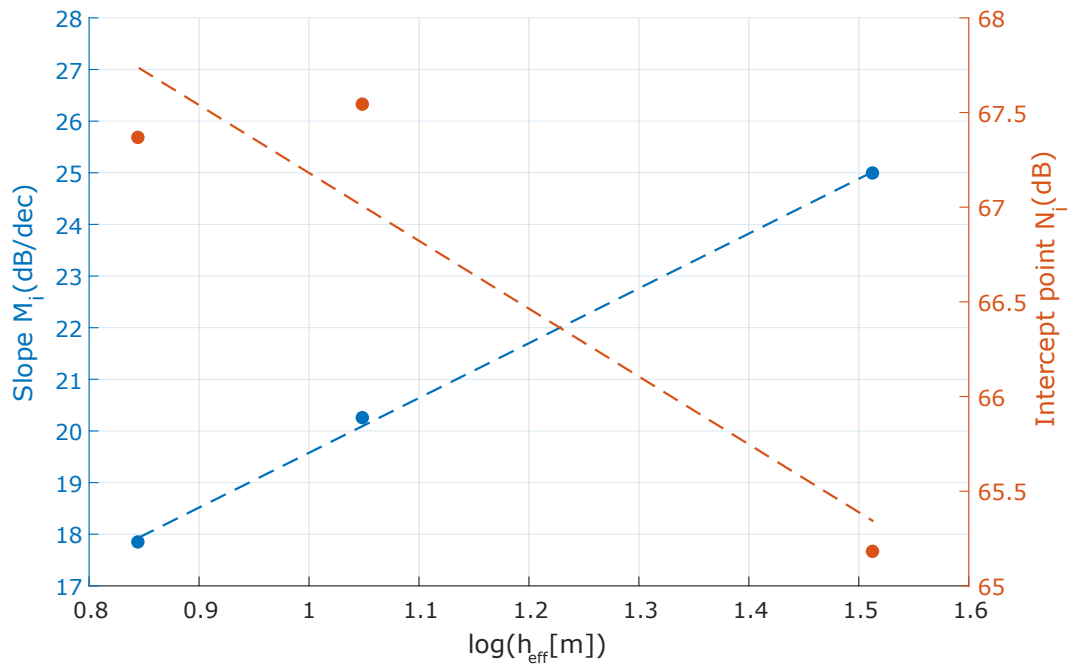


Figure 5.2 Slope and intercept point estimation using LS method.

5.2.3 Proposed path loss model

Once the different correction factors have been separately computed, the proposed expression for the path loss can be formulated as:

$$L(dB) = k + l \log_{10}(h_{eff}) + [p + q \log_{10}(h_{eff})] \log_{10}(d). \quad (5.18)$$

Considering the obtained values, the final equation is written as:

$$L(dB) = 70.7 - 3.6 \log_{10}(h_{eff}) + [9.0 + 10.6 \log_{10}(h_{eff})] \log_{10}(d), \quad (5.19)$$

which takes into account the effective height of the drone antenna, h_{eff} , and the link distance, d , in meters. This expression will provide a linear path loss behaviour once the h_{eff} is fixed to a certain altitude. On the one hand, the intercept point (*IP*) of this proposed model, will decrease at the same time the effective height increases. On the other hand, when the antenna is placed in higher locations, the slope (*SL*) of this model will increase. It is important to highlight that this model is only suitable for specific scenarios which fulfil some features. These characteristics are a distance range between 0 and 600 m, a drone antenna height between 7 and 35 m and a carrier frequency around 5580 MHz. The Fig. 5.3 shows the proposed path loss model tested at four different heights. Notice that the highest path loss contribution is achieved when the antenna is placed in the tallest position.

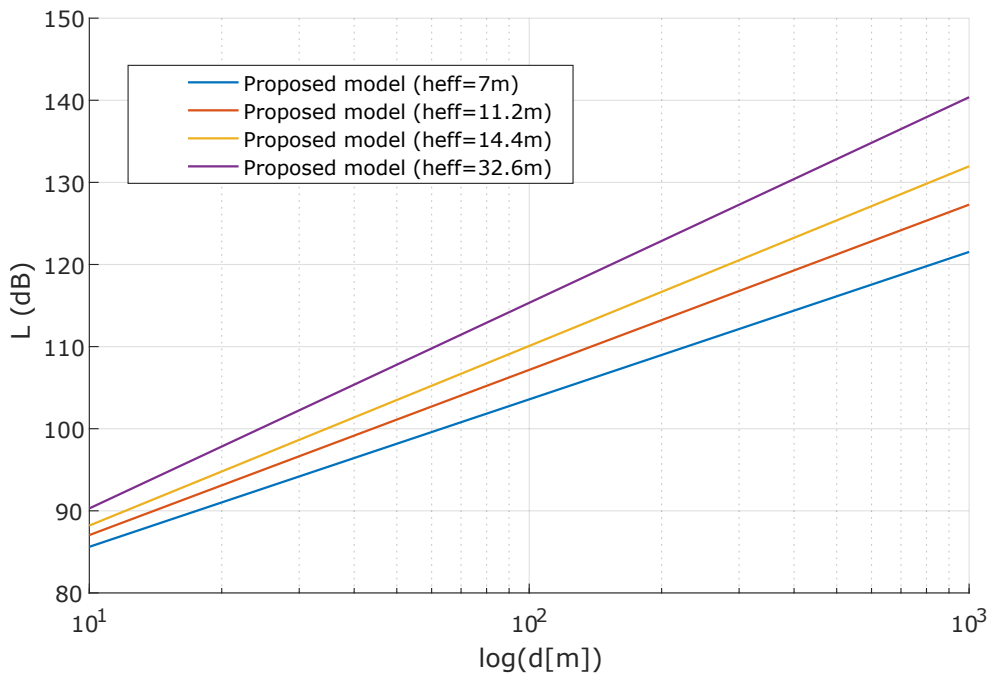


Figure 5.3 Proposed model with different effective antenna height (h_{eff}).

5.3 Proposed model verification

Once the new model has been implemented, it is important to analyse its performance and accuracy. As the proposed propagation model has used three sets of measurements of different scenarios, a good verification method is to apply this model to an independent set of measurements from a fourth scenario. This section will also study the error of the proposed model taking into account some methods explained in the Section 2.2.

Another measurement campaign has been performed in the suburban area of Hervanta, Finland. In this case, the drone antenna has been placed on the fourth floor of a building, at 13 meters from the ground level. These measurements have used the configuration described in Section 4.1. The Fig. 5.4 shows the locations where the system was tested. The drone antenna was located at the point X, of coordinates ($\phi_X = 61.44665969^\circ N$, $\lambda_X = 23.85291396^\circ E$). The ground station was testing the channel through 24 locations until achieving the point Y, of coordinates ($\phi_Y = 61.44738723^\circ N$, $\lambda_Y = 23.85483380^\circ E$), at 150 meters from the X position.

The fourth scenario considered an intermediate height compared with the scenarios A, B and C, placing the drone antenna on the fourth floor of a building, $h_D = 13m$. The average terrain height in this case, was 147.2 m over the sea level, providing

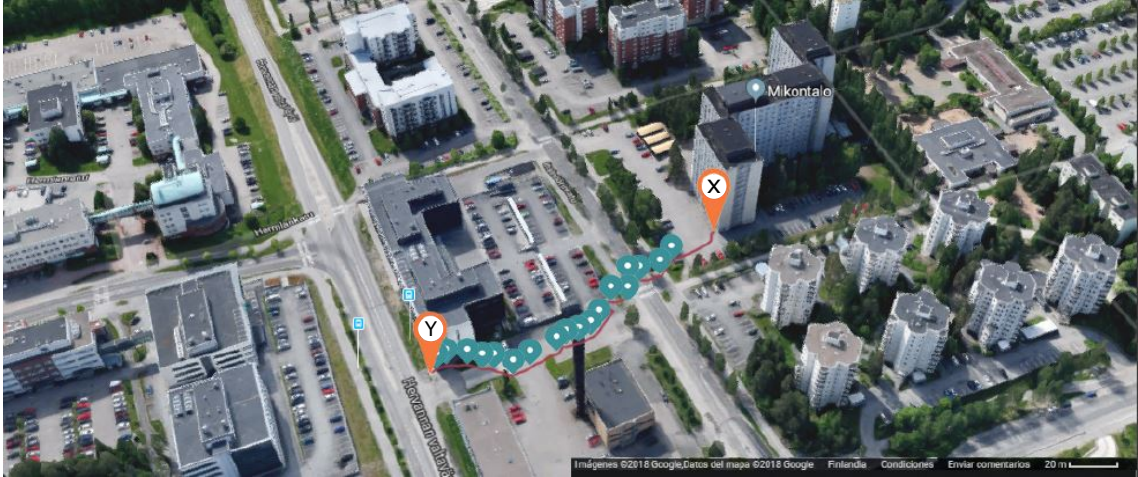


Figure 5.4 Measurements locations in scenario D with $h_D = 13\text{m}$. The figure is extracted from Google Maps [3] with its permission

an effective antenna height of $h_{eff,D} = 14,4\text{m}$. During these measurements, the antennas were placed at LOS locations providing a free first Fresnel zone which allows a good signal propagation. The elevation profile and the Fresnel zone of this scenario are presented in Fig. 5.5.

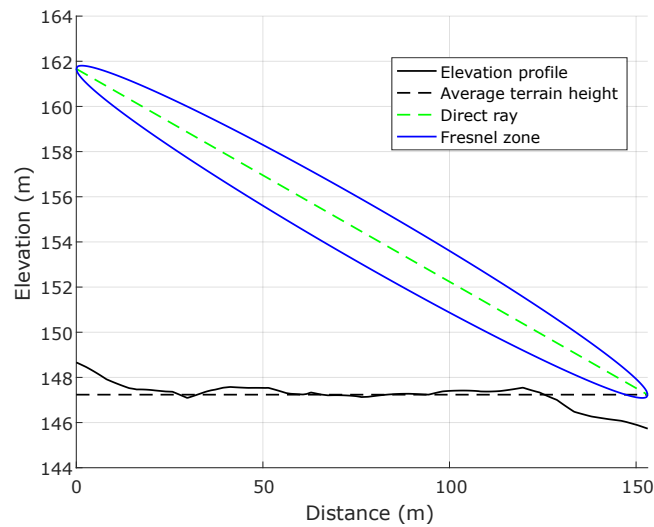


Figure 5.5 Elevation profile and first Fresnel zone at scenario D .

The received power has been measured in the drone antenna, providing the path loss results shown in the Fig. 5.6. The Least Squares method has also been implemented for this scenario in order to show the optimum function that approaches the loss measurements. Moreover, the proposed model is applied taking into account the expression 5.21 to the particular case of a link with an effective height of the drone

antenna of $h_{eff,D} = 14.4m$.

$$L(dB) = 70.7 - 3.6 \log_{10}(h_{eff,D}) + [9.0 + 10.6 \log_{10}(h_{eff,D})] \log_{10}(d) \quad (5.20)$$

Remarkably, the proposed model approaches the measured values with more accuracy when the distance between both antennas is larger. This scenario was tested for a shorter total distance of 150 meters compared to the distances of 600 and 250 meters of the previous scenarios.

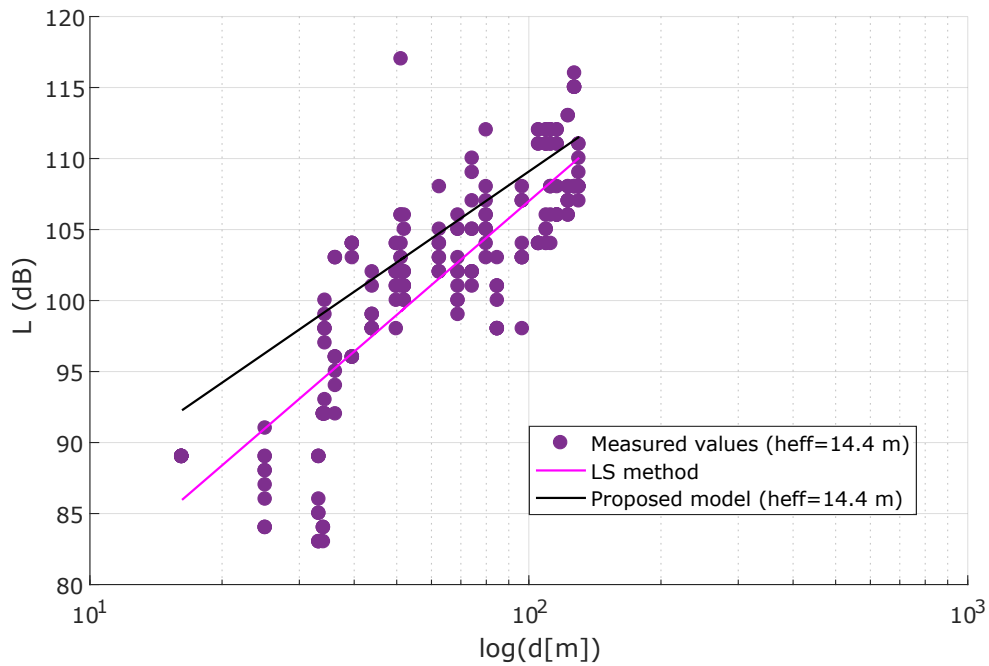


Figure 5.6 Proposed model analysis of scenario D, $h_{eff} = 14.4m$.

5.4 Error analysis

The final phase of the propagation modelling consists of the verification of the proposed model. For this purpose, it is necessary to measure how this model fits the empirical values obtained in each scenario. The Section 2.2.2 presented two different approaches to compute the error of a regression line optimization, the coefficient of determination (R^2) and the standard error regression (σ).

Then, the final proposed model with the expression 5.21 is applied to the four set of measurements as the Fig. 5.7 shows. This figure also presents the optimum function which approaches the measured values performed with the LS method. In the scenarios A, B and C, the proposed model (black function) shows almost the

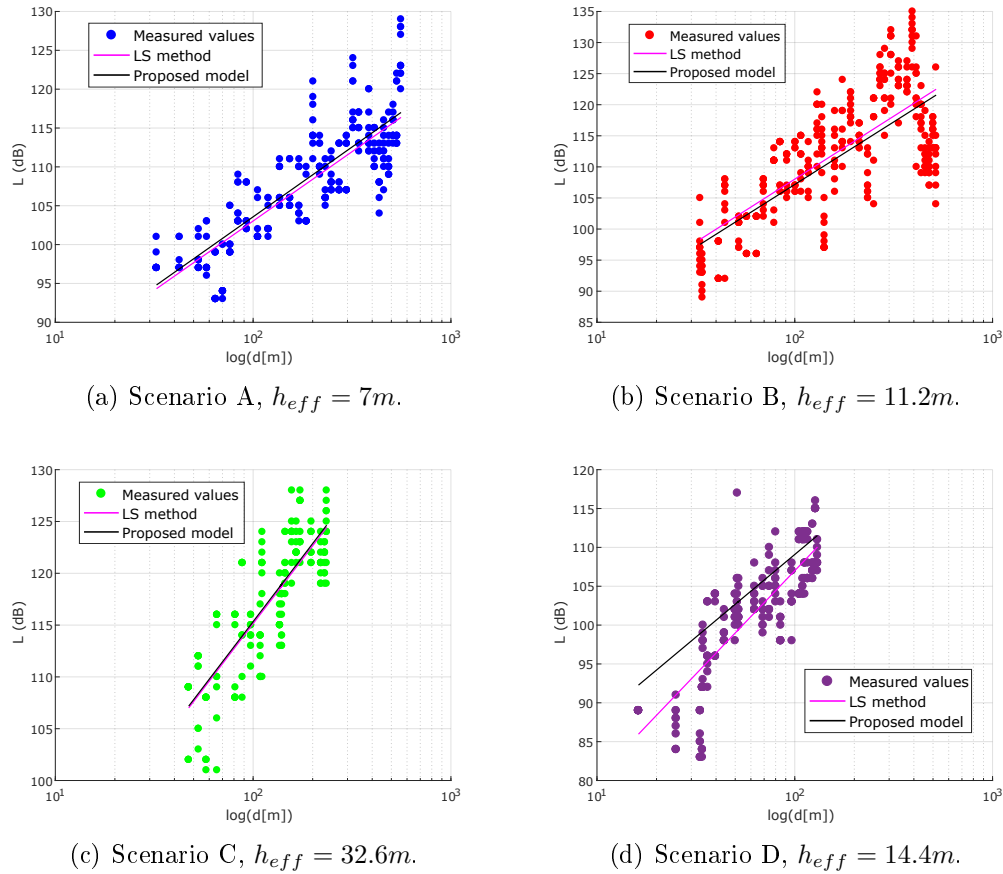


Figure 5.7 Proposed model compared to empirical measurements.

same behaviour as the LS method. This is because these set of measurements have been used to implement the propagation model. However, in the additional scenario D, the proposed model does not fit perfectly to the LS method. In this way, it is necessary to compute the residuals of this approximation. The residuals refer to the error between the predicted values by the proposed model \hat{L} , and the empirical measured data L . The Fig. 5.8 shows the error between these two variables in dB.

Taking into account these residuals, the coefficient of determination and standard error regression of each scenario have been computed. The scenario A presents a R^2 of 0.71 and a root mean squared error of 4.08. The scenario B shows a R^2 of 0.54 and a root mean squared error of 6.71. The scenario C shows a R^2 of 0.67 and a root mean squared error of 3.74. Notice that the scenario B presents the most dispersive behaviour as it is verified in Fig. 5.8(b). The additional scenario D presents a good fit with a R^2 of 0.70 and a root mean squared error of 4.26.

All the residuals have been unified in the same plot in order to show how the error is distributed. Then, an histogram has been implemented dividing the values of the

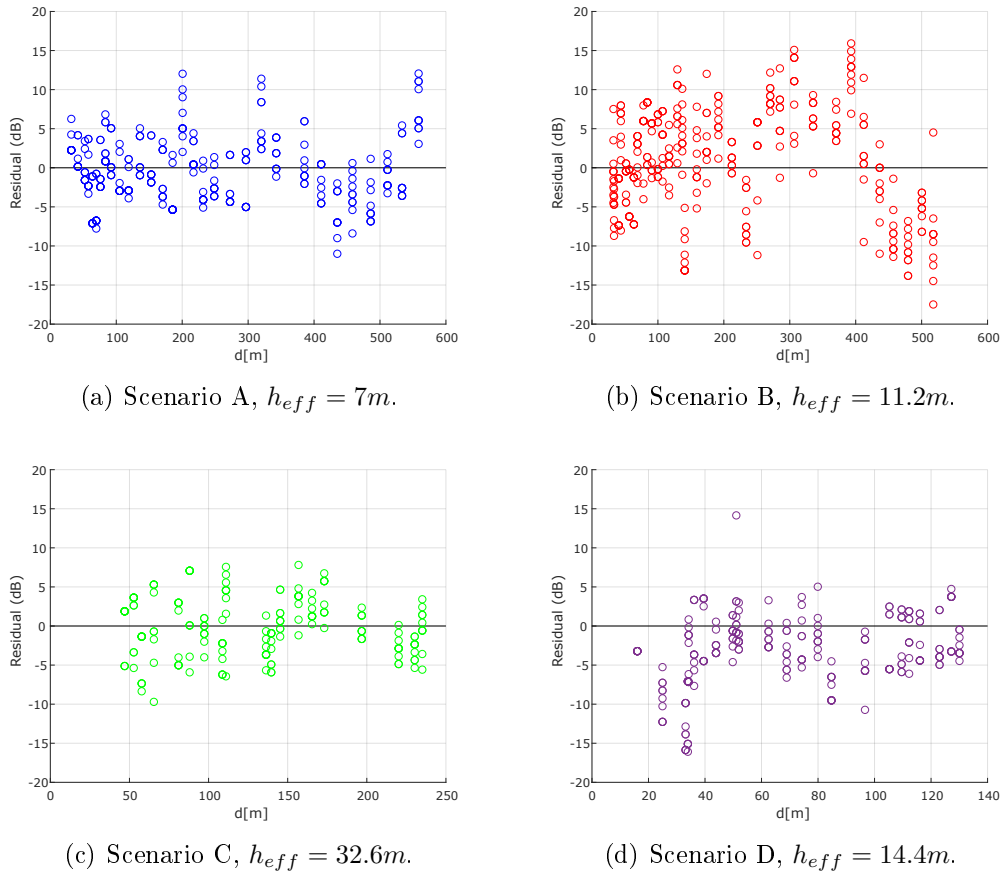


Figure 5.8 Residual plot from predicted model versus measured values.

residuals into 30 possible steps. The Fig. 5.9 shows how the probability density of the histogram describes a normal distribution. The histogram can be approached by a Gaussian random variable $X \sim \mathcal{N}(\mu, \sigma^2)$ with mean μ equals 0.6 and σ equals 5.3. Finally, the error distribution has been approached to a simpler Normal zero-mean distribution and σ equals 5, given by the random variable $X_\sigma \sim \mathcal{N}(0, \sigma^2)$ as it is shown in Fig. 5.9 in red.

Consequently, the propagation model is rewritten in order to consider the error deviation. The final expression is given as follows:

$$L(dB) = 70.7 - 3.6 \log_{10}(h_{eff}) + [9.0 + 10.6 \log_{10}(h_{eff})] \log_{10}(d) + X_\sigma \quad (5.21)$$

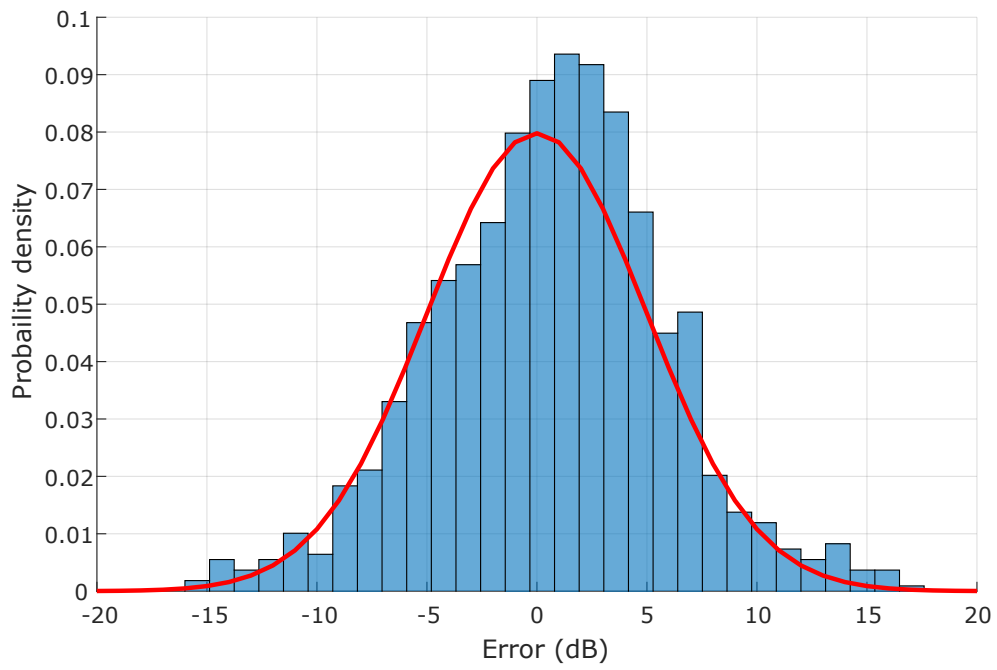


Figure 5.9 Probability density of the proposed model residuals.

6. CONCLUSIONS AND FUTURE WORK

This Master Thesis has developed a propagation model intended for air-to-ground communication links. The path loss between a ground station and a UAV can be analysed by means of the implemented propagation model. The measurement equipment has been set and calibrated in advance in order to present the desired path loss information. Based on empirical data obtained in three different LOS scenarios, a comparison is proposed to some well-known state of art models. However, none of the analysed models describes the path loss properly for this type of environment. Therefore, a new propagation model has been developed by a linear approach which considers a correction factor according to the UAV's height. This model is described by the following expression:

$$L(dB) = 70.7 - 3.6 \log_{10}(h_{eff}) + [9.0 + 10.6 \log_{10}(h_{eff})] \log_{10}(d) \quad (6.1)$$

The proposed model takes into account the effective height of the drone antenna, h_{eff} , and the link distance, d , in meters. This expression will provide a linear path loss behaviour once the h_{eff} is fixed to a certain altitude. As the model is based on a set of empirical measurements, it can only be applied in environments with a certain of features. These characteristics are a distance range between 0 and 600 m, a drone antenna height between 7 and 35 m and a carrier frequency of 5580 MHz. The performance and accuracy of the proposed model have been analysed considering a fourth set of measurements deployed with a different drone antenna height. It can be shown that the model fits correctly the empirical measurements, providing a standard deviation of 5 dB.

The evidence from this study suggests that the path loss in this type of link is considerably higher than the free space model, around 10-15 dB. However, it is shown that the empirical measurements present a similar trend to the free space case. The proposed model is limited by the linear approach that has been used, which can not consider the fluctuations that the measured data presents. Especially the scenarios with lower drone antenna heights showed periodic maximums and minimums similar to the 2-ray model. Therefore, to consider these effects, a more complex model could be studied in the future.

In this Master Thesis, the main emphasis was on implementing a propagation model to describe the path loss between a ground station and a UAV. For this purpose, empirical measurements have been made in a simplified scenario where the UAV height has been simulated placing one of the antennas in static locations whose height is similar to the flight drone altitude. Future studies should address how the path loss is affected when the antenna is mounted in the UAV. In this way, some aspects such the effect of the drone propellers or the antenna misalignment due to the UAV flight can be examined. Research into solving this problem is in progress, a customized drone has been implemented and set in order to allow automatic flights. Then, when the tracking system permits to point the antennas while the drone is flying, the same procedure followed during this Thesis will be repeated to tune the proposed propagation model with new set of measurements.

BIBLIOGRAPHY

- [1] “GCPX creating a gpx, pq or kml file from the coordinates,” <http://www.gcgpx.cz/?lang=en>, accessed: 2018-02-07.
- [2] “Geocontext geocontext-profiler,” <http://www.geocontext.org/>, accessed: 2018-02-07.
- [3] “Google Maps,” <https://maps.google.com/>, accessed: 2018-02-20.
- [4] “GPS - NMEA sentence information,” <http://aprs.gids.nl/nmea/>, accessed: 2018-02-20.
- [5] V. Abhayawardhana, I. Wassell, D. Crosby, M. Sellars, and M. Brown, “Comparison of empirical propagation path loss models for fixed wireless access systems,” in *Vehicular Technology Conference, 2005. VTC 2005-Spring. 2005 IEEE 61st*, vol. 1. IEEE, 2005, pp. 73–77.
- [6] A. Al-Hourani and K. Gomez, “Modeling cellular-to-uav path-loss for suburban environments,” *IEEE Wireless Communications Letters*, 2017.
- [7] R. Amorim, H. Nguyen, P. Mogensen, I. Z. Kovács, J. Wigard, and T. B. Sørensen, “Radio channel modeling for uav communication over cellular networks,” *IEEE Wireless Communications Letters*, vol. 6, no. 4, pp. 514–517, 2017.
- [8] Z. Arifin, M. R. Ibrahim, and H. R. Hatta, “Nearest tourism site searching using haversine method,” in *Information Technology, Computer, and Electrical Engineering (ICITACEE), 2016 3rd International Conference on*. IEEE, 2016, pp. 293–296.
- [9] J. Bardwell and D. Akin, “Certified wireless network administrator official study guide,” 2005.
- [10] I. Bucaille, S. Hethuin, T. Rasheed, A. Munari, R. Hermenier, and S. Allsopp, “Rapidly deployable network for tactical applications: Aerial base station with opportunistic links for unattended and temporary events absolute example,” in *Military Communications Conference, MILCOM 2013-2013 IEEE*. IEEE, 2013, pp. 1116–1120.
- [11] L. Canetta, G. Mattei, and A. Guanziroli, “Exploring commercial uav market evolution from customer requirements elicitation to collaborative supply network management,” pp. 1016–1022, June 2017.

- [12] M. do Vale, I. Gomes, G. Cavalcante, B. Castro, and F. Barros, “New terrain proposal for sui model equations based on 5.8 ghz measurements in wooded cities found in amazon region,” in *Antennas and Propagation (EUCAP), 2012 6th European Conference on*. IEEE, 2012, pp. 1187–1189.
- [13] S. Faruque, *Radio frequency propagation made easy*. Springer, 2014.
- [14] P. Finnegan, “World civil uas market profile and forecast 2017 edition,” *Teal Group Corporation*, 2017.
- [15] I. for Electrical and E. Engineers, “Ieee standard definitions of terms for antennas,” *IEEE Std 145-1993*, p. 40, 1993.
- [16] S. A. Glantz and B. K. Slinker, *Primer of applied regression and analysis of variance*, 1990, no. Sirsi) i9780070234079.
- [17] I. . B. W. A. W. Group *et al.*, “Channel models for fixed wireless applications,” 2003.
- [18] M. Hata, “Empirical formula for propagation loss in land mobile radio services,” *IEEE transactions on Vehicular Technology*, vol. 29, no. 3, pp. 317–325, 1980.
- [19] R. J. Hyndman and G. Athanasopoulos, *Forecasting: principles and practice*. OTexts, 2014.
- [20] *Scripting manual*, Mikrotik. [Online]. Available: <https://wiki.mikrotik.com/wiki/Manual:Scripting>
- [21] J. Milanovic, S. Rimac-Drlje, and K. Bejuk, “Comparison of propagation models accuracy for wimax on 3.5 ghz,” in *Electronics, Circuits and Systems, 2007. ICECS 2007. 14th IEEE International Conference on*. IEEE, 2007, pp. 111–114.
- [22] A. Orsino, A. Ometov, G. Fodor, D. Moltchanov, L. Militano, S. Andreev, O. N. Yilmaz, T. Tirronen, J. Torsner, G. Araniti *et al.*, “Effects of heterogeneous mobility on d2d-and drone-assisted mission-critical mtc in 5g,” *IEEE Communications Magazine*, vol. 55, no. 2, pp. 79–87, 2017.
- [23] J. D. Parsons, *The mobile radio propagation channel*. Wiley, 2000.
- [24] C. Thomas and W. Featherstone, “Validation of vincenty formulas for the geodesic using a new fourth-order extension of kivioja formula,” *Journal of Surveying engineering*, vol. 131, no. 1, pp. 20–26, 2005.

- [25] M. Valkama, “Basics of adaptative filtering with applications to communications receiver signal processing,” *Tampere University of Technology TUT* (*mikko.e.valkama@tut.fi*).
- [26] D. A. Weston, *Electromagnetic Compatibility: Methods, Analysis, Circuits, and Measurement*. Crc Press, 2016.
- [27] L. Yee Hui, F. Dong, and Y. S. Meng, “Near sea-surface mobile radiowave propagation at 5 ghz: measurements and modeling,” *Radioengineering*, vol. 23, no. 3, p. 825, 2014.
- [28] H. Zheng, W. Li, L. Tian, C. Xu, F. Huang, and J. Zhang, “Path loss models for urban macro cell scenario at 3.35, 4.9 and 5.4 ghz,” in *Personal, Indoor, and Mobile Radio Communications (PIMRC), 2015 IEEE 26th Annual International Symposium on*. IEEE, 2015, pp. 2229–2233.

A. APPENDIX

A.1 GPS coordinates algorithm

```

1 #1. Import packages
  import serial
3 import argparse

5 #2. Read serial port
  gps = serial.Serial("/dev/ttyUSB0", baudrate=9600)
7

  #3. Argument definition
9 parser= argparse.ArgumentParser(description='GPS coordinates')
  parser.add_argument('-i', help='Choose file number')
11 arg=parser.parse_args()

13 #4. Compute coordinates
  while True:
15     line = gps.readline()
      data = line.split(",")
17

      #Command GNRMC selection
19     if data[0]=="$GNRMC":
          if data[2]=="A":
21                 with open ("position.txt", "a") as pos:

23                         #Measurement ID
                          pos.write("Measurement; {}".format(arg.i))
25                         print("Measurement; {}".format(arg.i))

27                         #Measurement Latitude
                          pos.write(";Latitude; {}".format(data[3]))
29                         print(";Latitude; {}".format(data[3]))

31                         #Measurement Longitude
                          pos.write(";Longitude; {}\n".format(data[5]))
33                         print(";Longitude; {}\n".format(data[5]))

35                         break

```

A.2 Antenna measurement algorithm

```

#Option settings
2 :local testSamples 10;
  :local delaySamples 1;
4 :global testNumber;

6 #File creation
  :local fileName ($testNumber);
8 :local fileName ("range_test_" . $fileName . ".txt");
  /file print file=$fileName
10 /file set $fileName contents=""

12 #Variable definition
  :local signalStrength 0;
14 :local signalToNoise 0;
  :local fileContent("TEST ".$testNumber."BREAK;".id; signalStrength;
16                      signalToNoise; BREAK;");

18 #Measurement process
  :local x 1
20 :for x from=1 to=($testSamples) step=1 do={
  :foreach i in=[/interface wireless registration-table find] do {
22
    :put "Sample: [$x] "
24    :set fileContent ($fileContent . $x . "; ");

26    :set signalStrength [/interface wireless
                          registration-table get $i signal-strength];
28    :set fileContent ($fileContent . $signalStrength . "; ");

30    :set signalToNoise [/interface wireless
                          registration-table get $i signal-to-noise];
32    :set fileContent ($fileContent . $signalToNoise . "; ");

34    :set fileContent ($fileContent . " BREAK; ");
    :delay ($delaySamples)
36  }
  }
38

#Data saving
40 :put $fileContent
  /file set $fileName contents=($fileContent);

```

A.3 Haversine algorithm

```

1 %INPUTS
  % lat1: latitude of point 1 in degrees
3 % long1: longitude of point 2 in degrees
  % lat2: vector of latitudes in degrees
5 % long1: vector of longitudes in degrees
  % h1: antenna 1 height
7 % h2: antenna 2 height
  %OUTPUT
9 % d: vector with distance between coordinates 1 and 2 in meters
  % dp: vector with distance between antennas 1 and 2 in meters
11 function [d, dp] = Haversine (lat1, long1, h1, lat2, long2, h2)
    %Earth mean radius in meters
13     R = 6371e3;

15     %Latitude and longitude difference in rad
    dif_lat = (lat1-lat2)*pi/180;
17     dif_long = (long1-long2)*pi/180;

19     %Haversine formula
    a= (sin(dif_lat/2)).^2+cos(lat1*pi/180)*cos(lat2(1,:)*pi/180);
21     b= a.*((sin(dif_long/2)).^2);
    c= 2*atan2(sqrt(b), sqrt(1-b))

23     %Distance in meters
25     d=R*c;

27     %Distance height correction
    dp=sqrt((h1-h2)^2+d.^2);
29 end

```